Aerosol Remote Sensing Using AATSR

Haiyan Huang

Supervised by: R. G. Grainger

Postdoctoral Adviser: G. E. Thomas

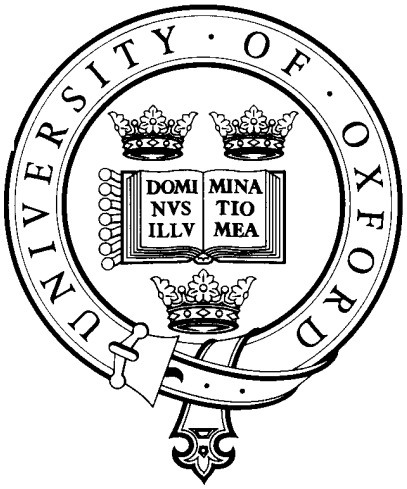

Transfer of Status Report

Trinity Term 2009

Atmospheric, Oceanic and Planetary Physics

Department of Physics

University of Oxford

Abstract

The following is a report of my activities in the first year of my D.Phil in atmospheric physics. Two major sections are presented. In the first section, the work on aerosol over remote ocean regions is discussed. A linear relation between aerosol optical depth (AOD) and wind speed is found by analyzing yearly data from two independent sources of AOD and wind speed. The second section focuses on the current and future projects on AATSR infrared aerosol retrieval algorithms . The report is organized as follows. In chapter 1, a brief review on atmospheric aerosol is given. A short description of aerosol measurement is explained in chapter 2. The newly found linear relationship between aerosol optical depth over remote ocean and wind speed using the data from AATSR is presented in chapter 3. The second part is aimed at improving the aerosol and sea surface temperature (SST) retrievals in infrared channels. Chapter 4 is about the work at present: atmospheric attenuation to the infrared radiance at top of atmosphere. A plan for future work and a timetable are included in chapter 5.

Contents

Chapter 1

Introduction

1.1 Atmospheric aerosol

Atmospheric aerosols are minute liquid or solid particles suspended in the atmosphere, with typical diameters ranging over four orders of magnitude, from a few nanometers to tens of micrometers. The life time of aerosols is about a few days to one week. Despite relatively short life times, aerosols regularly travel over long distances. The transport varies seasonally and interannually, demonstrating the global scope of aerosol influences. They exhibit a wide range of compositions and shapes that depend on their origins and subsequent atmospheric processes (Andreae and Crutzen [1997], Kulmala et al. [2000], Hildemann et al. [1991]). Pruppacher[1997] suggested dividing aerosols into different categories based on their sizes: the aerosol particles with diameters r $\leq$ 0.1 μm belong to the nuclei mode, particles with diameters 0.1 $<$ r $\leq$ 2.5 μm belong to the accumulation mode, all of these are defined as fine mode; particles with diameters r $>$ 2.5 μm are in the coarse mode. Figure. 1.1 shows the number and volume density distribution of aerosol. For many applications, aerosols from about 0.05 to 10 μm in diameter are of great interest, as particles in this size range dominate aerosol direct interactions with sunlight, and also make up the majority of the aerosol mass. Particles at the small end of this size range play a significant role in interactions with cloud, whereas particles at the large end, though much less numerous, can contribute

significantly near dust and volcanic sources. Over the ocean, giant salt particles may also play an important role in cloud development (Chin et al. [2009]).

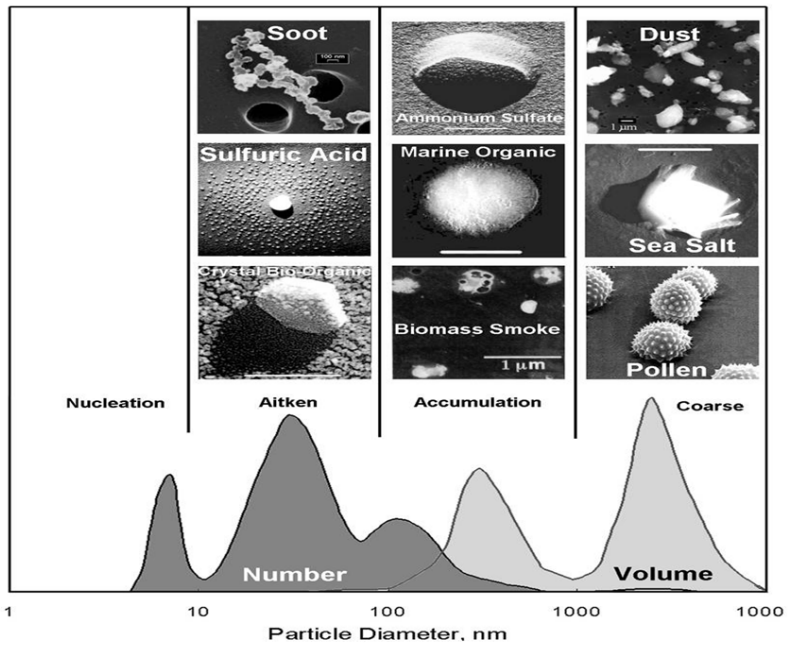

Figure 1.1: Number and volume density distribution of aerosol(Dahl [2005])

1.2 Source

Aerosol can either be produced by ejection into the atmosphere, or by physical and chemical processes within the atmosphere (called primary and secondary aerosol production respectively). Examples for primary aerosol are sea spray and windblown desert dust. Secondary aerosol are often produced by atmospheric gases reacting and condensing, or by cooling vapor condensation (gas to particle conversion), such as organic particles from oxidation of SO_2 . Figure. 1.2 shows some of these processes, along with the three size ranges where high aerosol concentrations are often observed, and the main process related to their growth and decay. The sources and sinks for the fine and coarse modes are different. The Table. 1.2 gives estimates about the annual global emissions of atmospheric aerosols.

Table 1.1: Global emission source strengths of main atmospheric aerosols, modified from Hinds [1999]

Source	range (Tg/yr)	Best estimate (Tg/yr)	Size mode
soil dust	1000 - 3000	1500	mainly coarse
sea salt	1000 - 10000	1300	coarse
volcanic ash	4 - 10000	30	coarse
biomass burning	3 - 150	20	fine
anthropogenic	320 - 640	460	mainly fine

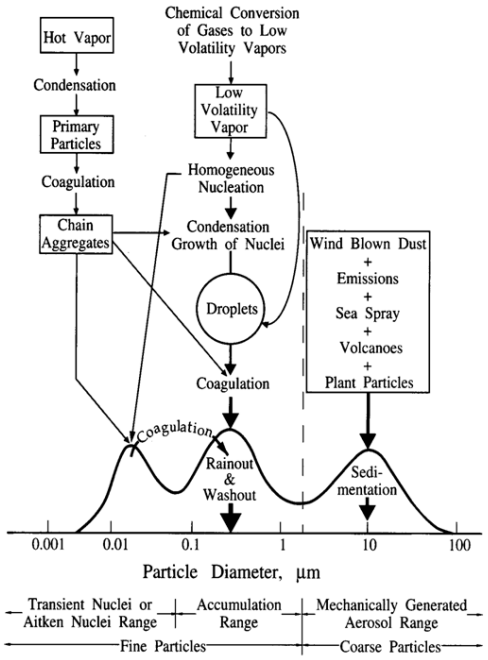

Figure 1.2: Idealized schematic of the distribution of surface area of an atmospheric aerosol. Principal modes, sources, and particle formation, and removal mechanisms are indicated Colbeck [1998]

1.3 Effect on climate

Aerosols exert a variety of impacts both directly and indirectly on the Earth's radiation and climate. The effects of aerosols have been widely studied (Charlson et al. [1992], Jacobson [2001], Haywood and Boucher [2000], Satheesh and Ramanathan [2000]). First, most of aerosols are highly reflective, they increase the albedo of the earth, thereby cooling the surface and effectively offsetting greenhouse gas warming by about 25% to 50% (Charlson et al. [1992], Kiehl and Briegleb [1993], Kaufman et al. [2002]). This is described as the direct effect. It makes the atmosphere brighter when viewed from space since much of Earth's surface is covered by dark oceans and aerosols also scatter visible light backing into space.

Secondly, aerosols in the low atmosphere act as sites at which water vapor can accumulate during cloud droplet formation, serving as cloud condensation nuclei (CCN). Any change in number concentration or hydroscopic properties of such particle has potential to modify physical and radiative properties of cloud. The indirect effects of aerosol include an increase in cloud brightness, a reduction in precipitation and an increase in cloud lifetime. The overall impact of aerosols is an enhancement of Earth reflectance (short albedo). Both of the effects are well described by Twomey [1977]. Aerosols also can act as sites where chemical reactions can take place (heterogeneous chemistry).

Finally, aerosols often contain black carbon particles which strongly absorb incoming sunlight. The effects of this type of aerosols are twofold: warming the atmosphere and cooling the surface below; reducing the atmosphere vertical temperature gradient and therefore contributing to the reduction of formation of convective cloud, this phenomenon is referred to the semi-direct effect. The IPCC 2007 aerosol forcing assessments are based largely on models. At present, aerosol influences are not yet quantified adequately according to Figure. 1.3.

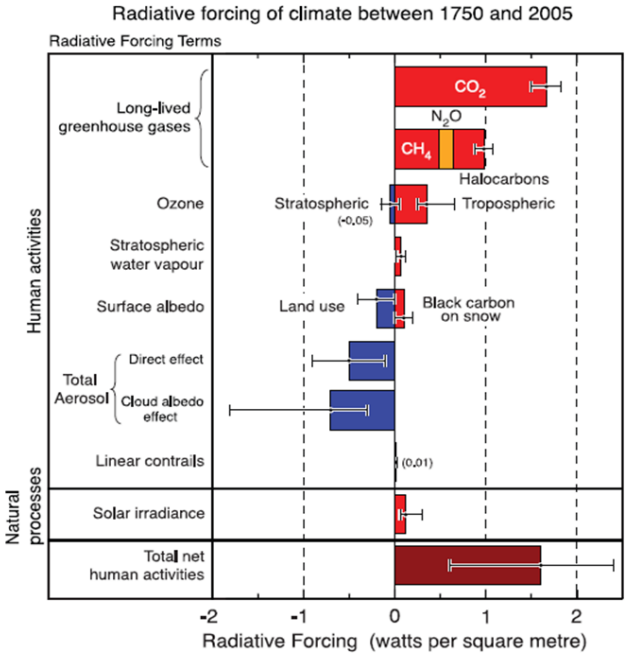

Figure 1.3: Global average radiative forcing (RF)estimates and uncertainty ranges in 2005, relative to the pre-industrial climate. The total anthropogenic radiative forcing and its associated uncertainty is also given(IPCC, [2007]).

1.4 Transport

Despite their relatively short average life times, aerosols indeed can travel over long distances. For example, particles moving at a mean velocity of 5 ms^{-1} and remaining in the atmosphere for a week will travel 3000 km (Chin et al. [2009]). Aerosols are dispersed though the processes of advection, convection and turbulence which is strongly dependent on seasons and meteorological background (Levin and Cotton [2009], Putaud et al. [2004], Ayers et al. [1991]). The best known examples are dust aerosols transported from Africa or Asia to the other continents (Duce et al. [1980], Prospero [2005]). As most aerosol sources are near the surface, aerosol concentrations are the greatest in boundary layer and remain confined to the troposphere, due to the lack of large-scale vertical mass exchange between troposphere and stratosphere. Large particles in particular rarely make their way from lower layers to high altitude because of the effect of gravitational settling, except violent volcanic eruptions

which are able to inject aerosols and precursor gases directly into the stratosphere. Deep convection also can transport air masses containing aerosols from anthropogenic and natural sources from the boundary layer into the upper troposphere in relatively short time scales.

1.5 Sink

Once aerosols are suspended in the atmosphere, they cannot stay there perpetually. The time spent in the atmosphere by an aerosol particle is a complex function of its physical and chemical characteristics as well as the time and location of release. The main sink mechanisms can be divided into two categories: wet deposition and dry deposition.

1.5.1 Wet removal

Wet deposition involves water and includes three sub calories: rain out, wash out, and sweep out. As mentioned above, aerosols can act as nuclei for condensation of cloud drops in clouds producing rain, those drops grow so large that they can fall to the ground in the form of rain drops. This is rain out. Rain out tends to be efficient over all size ranges due to the large surface area of cloud droplets and the rapid condensation of small particles especially for soluble particles. The distinction between rain out and wash out is that the wash out needs a pre-existing collecting droplet. Wash out is when an aerosol particle incorporates into an already existing cloud drop, and the drop grows large enough to fall as a rain drop. Wash out is more efficient for smaller particles. Both the rain out and wash out occur inside of cloud, while the sweep out happens below cloud layer. Aerosol remaining below the base of a rain cloud can be hit by falling drops and deposit itself within the raindrop. This mechanism is more effective for large size particles. These three processes are distinguished from each other because of the strong size and mass dependence. Wet deposition is also influenced by the amount of moisture.

1.5.2 Dry removal

The main difference between wet and dry deposition is that dry deposition does not require the aid of precipitation. Dry deposition is caused by many processes. Gravitational settling, which is dominated by the large particles, means aerosol falling under gravity. The terminal velocity of particles can be found by Stoke's Law (gravity is balanced by drag force). Settling velocity is proportional to particles mass, thus it is efficient for large particles. Figure. 1.4 shows the settling velocity of particles with different sizes at 298 K.

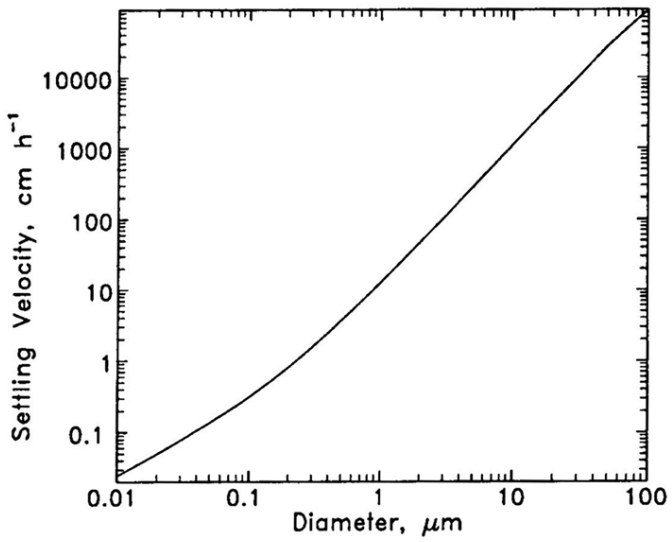

Figure 1.4: Settling velocity of particles in air at 298 K as a function of diameter, modified from Dahl [2005].

Diffusion, or Brownian motion, is the process by which aerosols move randomly due to the collision with gas molecules. It is only important for small particles. The distance of a particle diffuses in a given time can be calculated as

$$distance(cm) = \sqrt{Dt}, \tag{1.1}$$

where D is the diffusion coefficient. It decreases with the size of particle. Figure. 1.5 shows the diffusion coefficients of different diameters.

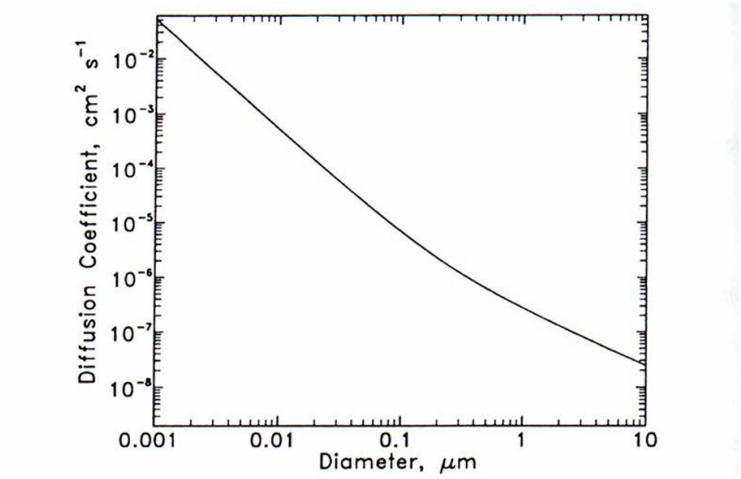

Figure 1.5: Aerosol diffusion coefficients in air at 293 K as a function of diameter, modified from Dahl [2005].

1.6 Parameters that describe aerosol microphysical and optical properties

Modeling the aerosol forcing on atmospheric radiation by solving the radiative transfer equation requires many aerosol optical properties: aerosol optical depth τ_λ(loading), phase function $p(\theta)$(angular dependence of light scattering), and single scattering albedo $\omega_0(\lambda)$ (ratio of scattering to scattering + absorption). The variations of the above optical properties determine the impact of atmospheric aerosol on climate change. Single scatter albedo determines the sign (cooling or heating, depending on the planetary albedo) of aerosol radiative forcing, while the others determine the magnitude of aerosol forcing (Hansen et al. [1997]).

1.6.1 Phase function

Phase function $p(\theta)$ describes the angular distribution of light reflected by a body when illuminated from a specific direction, where θ is scattering angle between the incidence and

scattering directions. The $p(\theta)$ is normalized to 4π by integration over all directions. It does not depend on the total number of particles. When polarization effect is considered, the phase function $p(\theta)$ is replaced by a 4×4 phase matrix $\mathbf{P}(\theta)$.

1.6.2 Extinction coefficient and Single Scattering Albedo

Extinction is the sum of scattering and absorption. The extinction coefficient K_e is defined as

$$K_e = K_s + K_a, \tag{1.2}$$

where K_s and K_a are the scattering coefficient and the absorption coefficient. The ratio of scattering efficiency to total radiation extinction is the single scattering albedo (ω_0). For spherical particles, the single scattering albedo can be calculated from Mie theory.

$$\omega_0 = \frac{K_s}{K_a + K_s}. \tag{1.3}$$

For non-absorbing particles, ω_0 is 1.

1.6.3 Aerosol optical depth (AOD)

AOD(τ) is a quantitative measure of the extinction of radiation by the column aerosol scattering and absorption between the aimed point and top of atmosphere. AOD typically decreases with increasing wavelength and is much smaller for long wave radiation than for shortwave radiation. Values of AOD(τ) vary widely depending on atmospheric conditions, but are typically in the range 0.02-0.2 for visible radiation.

$$\frac{L}{L_0} = e^{-m\tau} \tag{1.4}$$

Where $m = \cos\theta$, θ is the zenith angle and τ is the optical depth of atmosphere along this path. L_0 is radiance at the source and L is the observed radiance for a given path. It is the primary quantity obtained by satellite observation.

1.6.4 Effective radius

For a given type of aerosol, the size of particle determines the radiative effect. Effective radius (r_e) is a commonly used measurement of the average size of an aerosol distribution, defined as the ratio of the third and second moments of the size distribution.

$$r_e = \frac{\int_0^\infty r^3 n(r)\,\mathrm{d}r}{\int_0^\infty r^2 n(r)\,\mathrm{d}r}, \tag{1.5}$$

where r is the radius and $n(r)$ is the number distribution of aerosol particles as a function of radius, some studies such as (Davies [1974], Colbeck [1998]) have suggested the lognormal distribution to be most appropriate for atmospheric aerosol. For an aerosol distribution with mode radius r_m and total number density N_i, the number density $n(r)$ of particles larger than r in the distribution with spread s is given as follows,

$$n(r) = \frac{N_i}{\sqrt[2]{2\pi} r \log\sigma_i \ln 10} \exp[-\frac{1}{2}(\frac{\log r - \log r_m}{\log\sigma_i})^2]. \tag{1.6}$$

1.6.5 Ångström exponent

Ångström exponent is usually used to describe the dependence of aerosol optical depth (extinction coefficient) on wavelength.

$$\alpha = -\frac{\log\frac{\tau_\lambda}{\tau_{\lambda_0}}}{\log\frac{\lambda}{\lambda_0}}, \tag{1.7}$$

where τ_λ is the optical depth at wavelength λ and τ_{λ_0} is the optical depth at the reference wavelength λ_0. The Ångström exponent is inversely proportional to the size of the particle: the smaller the particles are the larger the Ångström exponent is. This relationship is useful in assessing the particle size of atmospheric aerosol.

1.7 Types of aerosol

Unlike the greenhouse gases, aerosols have a short life time and highly inhomogeneous spatial distribution which is strongly correlated to their sources. The impact of aerosols on

climate must be understood and quantified on a regional rather than a global basis. From observations from satellites, it is suggested the following types according to their possible sources.

1.7.1 Urban aerosol

Urban aerosols are mainly composed of fine hygroscopic particles and found in populated cities as well as their downwind regions. The loading of this kind of aerosols is highest in the northern hemisphere where industrial activities are centered. As shown by Figure. 1.7.4 and Figure. 1.7, north-east America, east Asia, and Europe are of high AOD but relatively low effective radius. The two important components of urban aerosol are sulphate and black carbon in fine mode. The sulphate aerosols absorb no sunlight but reflect it, thereby reducing the amount of sunlight reaching the Earth's surface. It is also closely related to the formation of acid rain. Absorption by black carbon is not only related to its concentration, but also dependent on its position relative to other aerosol particle, for example, absorption can be two to three times stronger if the black carbon is located inside the scattering particle. High concentrationed aerosols also enter cloud where they cause the number of cloud droplets to increase but make the droplet sizes smaller. The effect is to make the cloud reflect more sunlight making it hard for the CCN to grow to form the raindrop thereby prolonging the life time of the cloud (indirect effect).

1.7.2 Smoke from biomass burning

Smoke from vegetation fire, whether caused naturally or by humans, is widespread. The smoke from biomass burning is known as an absorbing aerosol with a high concentration of black carbon produced by combustion. The smoke is dominated by fine organic particles. Absorption is dependent on the vegetation type, flaming state, climate, the degree of aging of the particles, ambient temperature and relative humidity (Remer et al. [1998], Reid et al. [1999]). Although only 26% of the global land surface is located south of the equator, much

of it lies within or near the tropics, which is the area subject to most burning activities (Figure. 1.7.4 and Figure. 1.7). Dense smoke plumes are found annually downwind of fires in South America (August–October), Central America (April and May), Southern Africa (July–September) and Central Africa (January–March) (Kaufman et al. [2002]). The particle size distribution for smoke from above regions is dominated by accumulation mode (Figure. 1.7).

1.7.3 Dust

Dust, a the major types of troposphere aerosols, is emitted from dry lake beds and deserts in Sahara, East Asia, and Saudi Arabian deserts. The domination of large particles in desert dust aerosol is the principal feature differentiating the optical properties of dust from fine-mode dominated biomass burning and urban industrial aerosols (Dubovik et al. [2002]). Dust is brought into the atmosphere by saltation, a jumping motion whereby already detached, larger particles collide with obstructions on the surface bed, projecting smaller particles into the air. They are relatively large and would normally fall out of atmosphere after a short flight if they are not blown to relatively high altitudes (15,000 ft. or higher) by intense dust storms (Ginoux et al. [2001]). Due to their large size, dust particles absorb sunlight as well as scatter it, warming the layers where they stay. This warmer air is believed to inhibit the formation of storm clouds. Dust emission is influenced by large-scale air circulation, which affects flow from the continents, and drought conditions (Moulin [1997]). It is composed of large particles with varying concentrations of iron oxide that absorbs light in blue and UV wavelengths. However, African dust transported to Florida contains high concentrations of fine particles (10 - 100 gm^{-3}) during the summer months and exceeds local pollution standards on particulate matter. About 50% of this is subject to long-range transport and will turn up all over the world. Saharan sand is thought to play a vital role in the support of vegetation in the Amazon basin and provides nutrient iron to the biochemical cycle of the ocean systems.

1.7.4 Marine aerosol

Marine aerosol is composed of coarse salt particles generated from bursting sea foam in windy conditions and fine sulphate particles and organic species, formed by gas to particle conversion processes such as binary homogeneous nucleation, heterogeneous nucleation and condensation (O'Dowd et al. [2001], Fitzgerald [1991]). An important characteristic of marine aerosol is the substantially low optical thickness compared to desert dust, as well as to urban industrial and biomass burning aerosols. High sea salt levels are located at high latitude bands near 60°S and 60°N. The marine aerosols play important roles in radiation and climate by absorption and scattering. In addiction, marine aerosols effect the droplet size distribution and albedo of marine boundary layer cloud and sulphate cycle in the marine environment. Marine aerosol generally absorb very little sunlight, thus its AOD is estimated to average 0.07 at 550 nm in most regions, but increases in windy region south of 40°S to 0.2 (Chin [2002]).

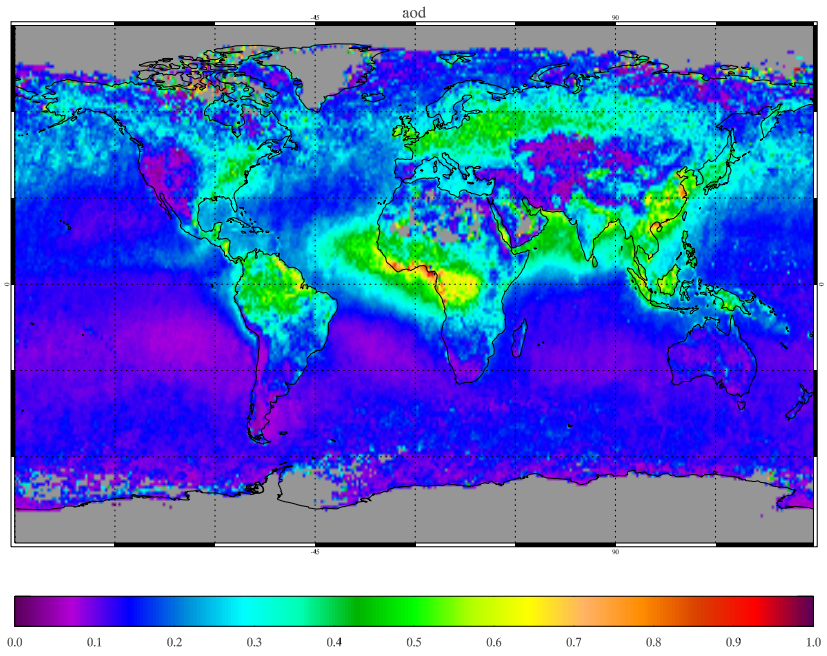

Figure 1.6: Annual average aerosol optical depth at 550nm for 2004, AATSR

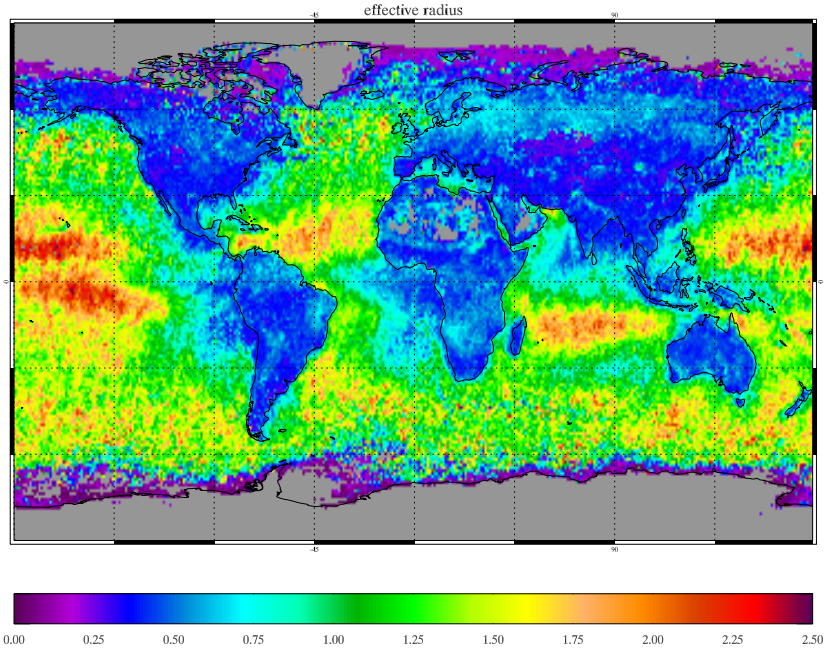

Figure 1.7: Annual average effective radius for 2004, AATSR

Chapter 2

Measurement of Aerosol from Space

One of the greatest challenges in studying aerosol impacts on climate arises from the large spatial and temporal heterogeneity of aerosol concentration, chemical composition and size. The tools for measurement of aerosol include *in situ* measurements from the ground and remote sensing from space. The measurements of aerosol on a global scale can be realized only through satellite remote sensing, which is the only means of characterizing the large and temporal heterogeneities of aerosol distribution (Chin et al. [2009]).

2.1 Overview of aerosol measurement from space

Monitoring aerosols from space has been performed for more than two decades. Table. 2.1 summaries major satellite measurements currently available for aerosol characterization and research. Early aerosol monitoring from space relied on sensors that were designed for other proposes, such as AVHRR and TOMS, which were originally intended for cloud, surface and ozone properties respectively. They used ultraviolet, visible, infrared and micron channels. These channels are also sensitive to absorption and scattering of aerosol particles. Satellites measure the angular dependence of radiance and polarization at multiple wavelengths and angles at fine spatial resolution. The aerosol products include optical depth, information about particle size, phase function. The accuracy for AOD measurement is about 0.05 or

20 % of AOD and is better over dark surface (ocean), but that for aerosol microphysical properties, which are important distinguishing aerosol types, is generally low. However, the accuracy of AOD is still poorer than that from surface-based sun photometers by 0.01 to 0.02, even over dark oceans.

2.2 Introduction of AATSR

The Advanced Along-Track Scanning Radiometer (AATSR) is one of the Announcement of Opportunity (AO) instruments on board the European Space Agency (ESA) satellite ENVISAT, launched in March 2002, a following on from ATSR-1 and ATSR-2 on board ERS-1 and ERS-2, which were launched in July 1991 and operated until Match 2000 and in April 1995 and is expected to continue to operate at least until the end of the ENVISAT commissioning phase respectively. Thus this family of instruments will establish a unique long term data set supporting not only ocean and climate research, but also a wide range of land surface and atmospheric applications including cloud, precipitation and aerosol. The bulk of instrument technical information and figures in this chapter are taken from official AATSR reference documents by ESA [2007].

2.2.1 Geometry of AATSR

The AATSR is onboard of ENVISAT. ENVISAT is designed for a sun-synchronous polar orbit, with a mean local solar time of 10:30am for the descending node, which optimizes illumination conditions for the optical instruments. The operating altitude is approximately 800km and 98.55° inclination to the equator. The nominal orbit has a repeat cycle of 35 days and an orbital period of about 101 minutes.

The AATSR and its predecessors are unique because they use two views (near simultaneous in time) with different path lengths to discriminate between radiance from the surface and radiance from the atmosphere. The target is first viewed along the direction of the orbit

Table 2.1: Summary of major satellite measurements currently available for observation of aerosol, modified from King et al. [1999] and Chin et al. [2009]

Instrument	Year coverage	Spatial coverage	Main Parameters
AVHRR/NOAA-series	1981-present	daily, global ocean	angstrom exponent, optical depth
TOMS/NIMBUS, ADEOSI	1979-2001	daily, global land and ocean	optical depth,absorbing index, single-scattering albedo
MODIS/TERRA, AQUA	2000-present	daily global land and ocean	optical depth, fine-mode fraction, angstrom exponent, effective radius and asymmetry factor (only for ocean)
MISR/TERRA	2000-present	global land and ocean	angstrom exponent, optical depth, small, medium, large fractions, non-spherical fraction
OMI/AQUA	2005-present	daily, global land and ocean	optical depth, absorbing aerosol index, single-scattering albedo, absorbing optical depth
MERIS	2002-present	global land and ocean	angstrom exponent, optical depth
POLDER-1, -2, PARASOL	1997-present	global land and ocean	angstrom exponent, optical depth, fine-mode fraction, non-spherical fraction
SeaWiFS	2004-present	global ocean	angstrom exponent, optical depth
SEVIRI	2004-present	global land and ocean	angstrom exponent, optical depth
GLAS/ICESat	2003-present	global land and ocean	extinction/backscatter
CALIOP/CALIPSO	2006-present	global land and ocean	extinction/backscatter,color ratio, depolarization ratio
AATSR	2002-present	global land and ocean	angstrom exponent, optical depth, effective radius

track, at an angle of 55°, as the spacecraft flies forwards the scene. Then, 120 seconds later, or when the satellite has moved approximately 1000 km forward along the ground track (forward view), a second observation is made of the same scene at the sub-satellite point (nadir view), as shown in Figure. 2.2.1

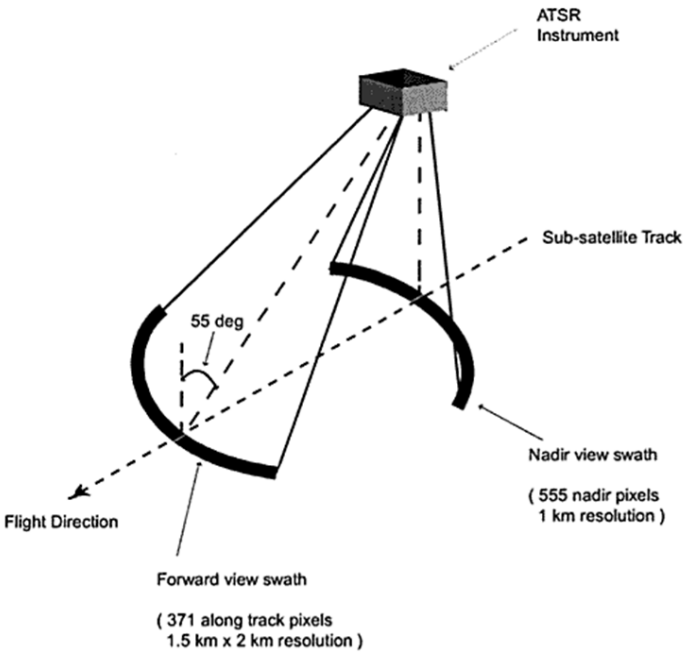

Figure 2.1: (A)ATSR viewing geometry

2.2.2 Instrument swath

The AATSR field of view comprises two 500 km wide curved swaths, with 555 pixels across the nadir and 371 pixels across the forward swath, as shown in Figure. 2.2.2. The scan cycle is repeated 6.6 times per second and the sub satellite point on the earth's surface moves forward by 1km during each scan cycle.

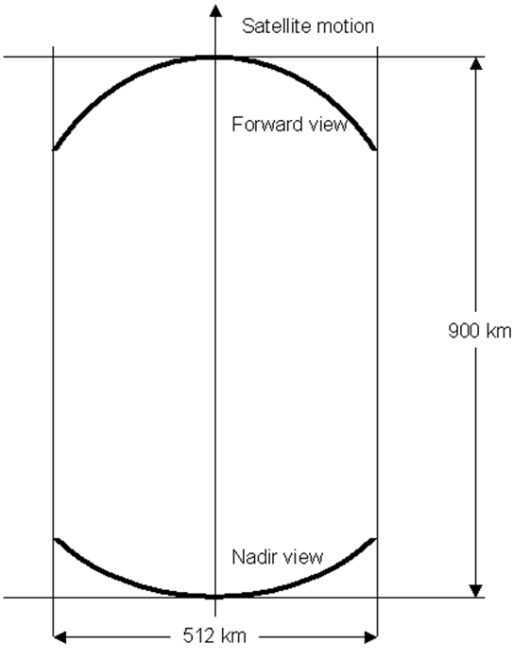

Figure 2.2: AATSR swaths

2.2.3 Special features of AATSR

Unlike the ATSR-1, which measured radiance at three channels in the infrared part of the spectrum, ATSR-2 and AATSR have four channels in the visible region plus the three infrared channles, as shown in the Figure. 2.2.3. Those visible channels are the key to the instruments' ability to provide data suitable for aerosol retrievals. AATSR is an improvement on ATSR-2 in this way: ATSR-2 suffers from restrictions on the amount of data which can be down linked while AATSR is able to provide continuous data from all channels.

2.3 The uses of AATSR data

AATSR data provide information on surface temperature, clouds, aerosols, vegetation, and snow cover in addition to calibrated, reference radiances and imagery.

Channel	Central Wavelength	Bandwidth
0.55µm	0.555µm	20nm
0.66µm	0.659µm	20nm
0.87µm	0.865µm	20nm
1.6µm	1.61µm	0.3µm
3.7µm	3.75µm	0.3µm
11µm	10.85µm	1.0µm
12µm	12.00µm	1.0µm

Figure 2.3: Spectral positions of AATSR channels

2.3.1 Sea Surface Temperature

The main objective of AATSR is to provide highly accurate sea surface temperature for the general climate model.

Ocean surface is considered to be an emitter of radiation with a peak in emission at around 10 μm, and the region between 10 and 13 μm is a suitable window with both low atmospheric absorption and good radiance sensitivity to small changes in sea surface temperature. The AATSR channels at 11 and 12 μm are selected for the retrieval of SST. The 3.7 μm is also used to provide an additional channel at night time, because the measurement at 3 - 5 μm is affected by solar radiance during daytime. They show very high radiometric sensitivity at night. The 1.6 μm channel is used to cloud flag and the others are used to correct atmospheric absorptions (the basis of aerosol retrieval). Retrieved AATSR dual view SST values achieve an absolute accuracy of better than $\pm$ 0.3 K, and up to 0.1 K under favorable conditions. The derived AATSR SST values are estimated from algorithms based on radiative transfer models, for example (Minnett [1990], Zavody et al. [1995]) , which

perform a linear or nonlinear regression of SST to simulated brightness temperatures (BT) with nominal band centers located at 3.7 μm, 11 μm and 12 μm, utilizing either the nadir view or a combination of the nadir and forward views offered by the instrument.

2.3.2 Land surface remote

Visible and near infrared channels were added to AATSR to enable land surface remote sensing. Compared with the ocean, the difficulties in remote sensing over land include the strong dependence of land surface albedo on viewing geometry; it has a steep bi-directional reflectance distribution function (BRDF), which makes modeling more difficult and the high heterogeneity over the scale of instrument resolution-adjacent fields of different crops can have very different albedos. Despite those difficulties, the land surface temperature and vegetation properties, which are routinely retrieved except for sun glint regions. (North et al. [1999], North [2002])

2.3.3 Cloud and aerosol retrieval

Absorption of aerosol is generally spectrally and angularly dependent. The multi - channel and dual-view features offered by AATSR are a powerful combination for cloud and aerosol investigations. Oxford-RAL Aerosol and Cloud (ORAC) is a scheme for aerosol and cloud retrievals, developed by AOPP and the Rutherford Appleton Laboratory (RAL). The principles behind aerosol and cloud retrievals are similar in that aerosol may be considered to be a very optically thin layer of cloud. Cloud parameters retrieved by ORAC include optical depth, effective radius, cloud-top temperature, the fraction of cloud within a pixel or superpixel, and cloud type. Cloud-top temperature may be converted to height and pressure. Aerosol parameters include optical depth, effective radius and angstrom exponent. The retrieval of aerosol in visible and near infrared channels is discussed in details by (Thomas et al. [2007], Sayer [2008])

Chapter 3

Aerosol Properties in the Remote Ocean

Natural aerosols are of particular importance because they provide a kind of base level of aerosol impact, and there is no effective way to control them, unlike their anthropogenic counterparts. On the global scale, the abundance of natural aerosols is several times greater than that of anthropogenic aerosol. The main natural aerosols include dust, volcanic ash, sea salt, natural sulphate and those from natural forest fire. As mentioned above, aerosols in the marine atmospheric boundary layer are comprised mainly by sea salt and organic particles related to the biological activities of ocean creatures. Therefore, the factors influencing the properties of sea salt or organic aerosol would have impacts on the properties of marine aerosol. There are three factors that would influence the optical properties in marine environments: relative humidity, the chemical interaction of oceanic biology and wind.

Relative humidity (water vapor content) is important for the growth of aerosol particles. In the coastal and marine environment, the aerosol are substantially hygroscopic, the water soluble fraction contribute much to the optical depth. These particles would undergo significant changes in their size, density and refractive index associated with changes in the atmospheric water vapor content. Studies have shown a significant increase in particle size and mode size with increase in relative humidity (Nair and Moorthy [1998], Lewis and

Schwartz [2004]). And generally, aerosol optical depth increases with increasing relative humidity, but sometimes the effect would be masked by the other factors, such as wind.

Oceanic emission of Dimethyl sulfide (DMS) is important because of its role as a precursor of atmospheric sulfate aerosol, it is also a useful factor for studying the transfer between air and sea. DMS is oxidized by free radicals that contain oxygen (such as NO_3^{-1} and OH^-) to SO_2 and sulfate aerosol. Sulfate aerosols act as the main source of cloud condensation nuclei over oceans.

Wind has two effects on the marine boundary layer (MBL) optical properties: the local effect and the long transport effect. Wind blowing over the sea surface produces the sea salt aerosol, which has an important influence on many processes in the MBL, while the wind from main continents can take the aerosol emitted by the land sources into the oceans. The long transport effect often matches the synoptic wind field well. This effect is very obvious in the near sea regions, such as the coast line of northern Africa and East Asia (Wai and Tanner [2004]).

3.1 Sea salt aerosol and wind

Sea salt aerosol is defined as the aerosol component consisting of sea water drops and dry sea salt particle. It carriers of species containing Na, Cl, Br, I and S. The particles are produced at the ocean surface by the bursting of bubbles resulting from the entrainment of air induced by wind stress (Fitzgerald[1991]; O'Dowd et al.[1997]). In undisturbed marine environment, far from continents and anthropogenic sources, it is often the dominant aerosol type, with a significant fraction occurring in the sub micrometer size range. Additionally, sea salt is one of the major contributors to the mass of particulate matter injected into the atmosphere globally and also links to chemical reactions in MBL. Sea salt aerosol with diameter near 5 μm can provide a strong CCN source and it can be involved in a climate feedback mechanism if wind speed is going to increase with global warming. Due to their lower activation threshold than that of a similar size sulphate particle, the sea salt can

comprise more than 90 % of active CCN in marine stratocumulus, even in sulphate rich air masses (O'Dowd et al. [2001], Fitzgerald [1991], Gras and Ayers [1983], Heintzenberg et al. [2003], Hoppel et al. [1990], Clarke et al. [2003]). Sea salt affects climate by scattering of solar radiation. It contributes 44 % to the global aerosol optical depth. According to IPCC 2001, the global annual radiative forcing due to sea salt are -1.51 and -5.03 Wm^{-2} for low and high emission.

The measurement of pure sea salt size distribution as a function of wind speed is quite difficult due to the large range of particles size encountered and the very low concentration present in larger sizes. Sea salt number and mass concentrations are strongly dependent on wind speed, typically adhering to exponential relationship in the form of $\log C = aU_{10} + b$, where C is the concentration, U_10 is the 10–meter wind speed, a and b are constants which depend on particles size (Exton et al. [1985], O'Dowd and de Leeuw [2007], Andreas [1998]).

Figure. 3.1 illustrates the observed size distributions normalized to 80% relative humidity at different wind speeds.

Mostly, the source functions are presented as power law functions and hence, at higher wind speeds, the production of sea spray increases in greater proportion than the wind speed increase.

The effect of wind on aerosol over the oceans has been studied, but has mostly focused on the aerosol concentration and size distribution. Definite correlation was found between surface wind speed and sea salt aerosol concentration (O'Dowd and Smith [1993], Nilsson et al. [2001], McDonald et al. [1982]). The influence of wind speed on aerosol optical depth, τ, in the atmosphere is a much more difficult problem (Platt and Patterson [1986], Villevalde et al. [1994], Smirnov et al. [1995], Moorthy et al. [1997]). The link between marine aerosol optical properties and wind speed is not easy to quantify because it can be masked by long range aerosol transported from land based sources. Thus oceanic regions far from continents with no or less influence of long range transport is important for studying such a relationship.

(Smirnov et al. [2003]) reported that aerosol optical depth measured at Midway Island, located in the northeastern Pacific Ocean at 28.12° N and 177.22° W, has a weakly correlated

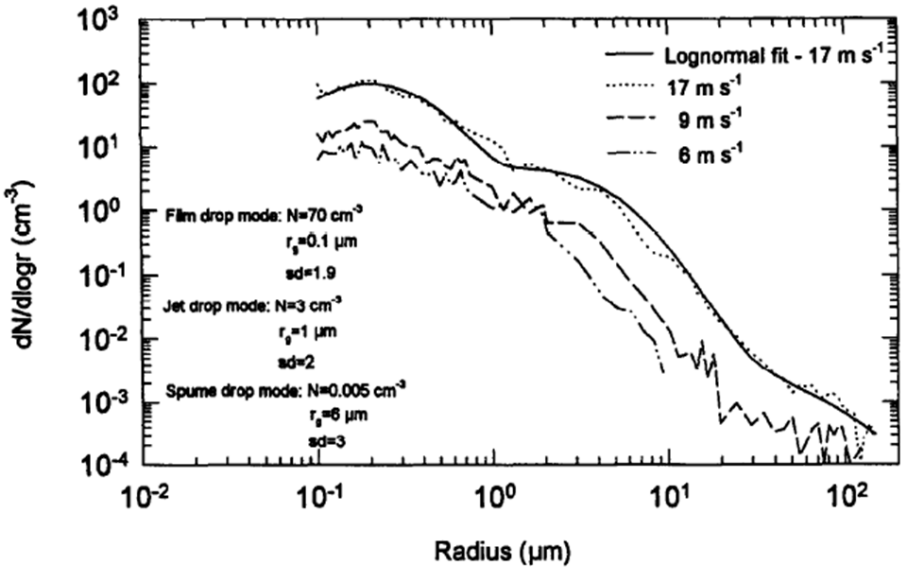

Figure 3.1: sea-salt size distributions at 6, 9 and 17 ms^{-1} and fitted log-normal distribution (O'Dowd et al. [2001].

)

linear relationship with 24-hour average surface wind speed. Other studies have also reported similar relationships. (Jennings et al. [2003], Smirnov et al. [1995], Villevalde et al. [1994]) Moorthy and Satheesh [2000] found an exponential increase in daily averaged aerosol optical depth with wind speed at the island of Minicoy in the Arabian Sea. However, the region of this study is close to land so that it cannot be considered as a pristine marine environment. Mulcahy et al. [2008] obtained a power-law relationship between wind speed and aerosol optical depth at four different wavelengths at Mace Head, located on the west coast of Ireland. This site is similarly not representative of the remote ocean. Based on one month of τ data from the Sea-viewing Wide Field-of-view Sensor (SeaWiFS) and surface wind data from ECMWF, Glantz et al. [2009] found a power-law relationship between surface wind speed and aerosol optical depth for the north Pacific. However, in their study, a single surface reflectance value was used in the retrieval of aerosol optical depth from SeaWiFS. The influence of white caps generated by enhanced wind speed could cause spurious backscatter

and influence the retrieved aerosol loading.

Though many studies have been performed, there is still no consensus on the relationship between wind speed and the observed aerosol optical depth. Additionally, all of the previous studies were from different locations using different instruments and in different time periods. Hence a direct comparison between their results is difficult to make and it is hard to extrapolate their results to other areas. Also, some locations where the experiments were carried out are close to continents. It is hard to apply those results to other places. In this work oceanic areas where can be taken as remote ocean are determined, based on the wind directions and aerosol optical depth , and then the relationship between aerosol optical depth and wind speed over the remote ocean regions, where the influence of continental aerosols can be considered minimal, is investigated. The paper is organized as follows: In Section 3.2, the data and the instruments used are briefly explained; a quantitative method to distinguish remote oceanic regions from areas influenced by continental outflow is introduced in Section 3.3. Preliminary results are presented in Section 3.4; concluding remarks are given in Section 3.5.

3.2 Data

Aerosol data used in this paper were the aerosol optical depth at 550 nm, τ, retrieved from Advanced Along-Track Scanning Radiometer (AATSR) as part of the ESA Globaerosol project (Thomas et al. [2008]). AATSR is on board the European Space Agency's Envisat platform, which is in a sun synchronous orbit with an overpass time of 10:30 a.m. local solar time. AATSR acquires two near-simultaneous observations of the same area of the Earth's surface at a viewing angle of 55° (forward view at the surface) and then approximately 90 seconds later at an angle close to vertical (nadir view). The dual-view allows AATSR to retrieve surface reflectance and τ independently (Sayer [2008]). The changes in surface reflectance do not influence the precision of the τ retrieval. The data used in this paper have a resolution of $1^\circ \times 1^\circ$, and are obtained daily for the whole year of 2004 over the global oceanic regions. The 10-meter wind from ECMWF is used in this paper at the same spatial

resolution as the τ data. The wind fields at has been interpolated to nominal local Envisat over pass time. Based on zonal (u) and meridional (v) wind components given by ECMWF, the wind speed (s) is calculated using $s = \sqrt{u^2 + v^2}$ and wind direction is defined as shown in Figure. 3.2b.

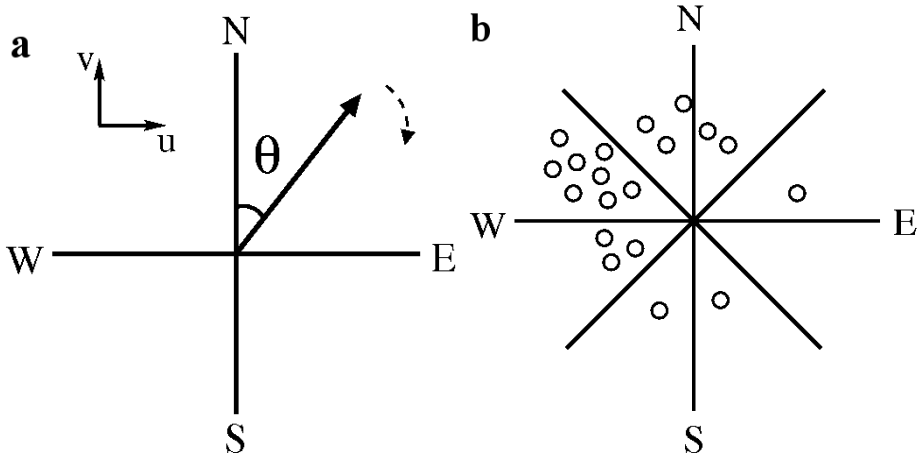

Figure 3.2: (a). Definition of wind direction. (b) τ daily data (indicated by the circles) are categorized by wind direction.

3.3 Method

To get a clear understanding of the relation between wind speed and τ, the first step is to define the remote ocean regions. A heuristic argument that can be made that, for truly remote oceanic regions, the only aerosol source is the ocean and thus it can be concluded that the τ should not depend on wind direction but only on wind speed and other parameters such as temperature. For each $1^\circ \times 1^\circ$ point in the global ocean, the daily τ data are sorted into different bins according to the corresponding wind direction. Figure. 3.2b illustrates a simple example with only 8 bins chosen. In practice, thirty six 10° bins are used and then calculate the average value of τ in each bin and the standard deviation of the average value over all wind directions σ_τ. The value of σ_τ indicates the dependence of τ on wind direction. If σ_τ is large, τ at the this point changes markedly as the wind direction changes, indicating that a possible external source of aerosol exists. On the other hand, if the σ_τ is small, τ

shows no dependence on wind direction, indicating that the corresponding area is a possible pristine oceanic candidate. This is shown stylistically in Figure. 3.3.

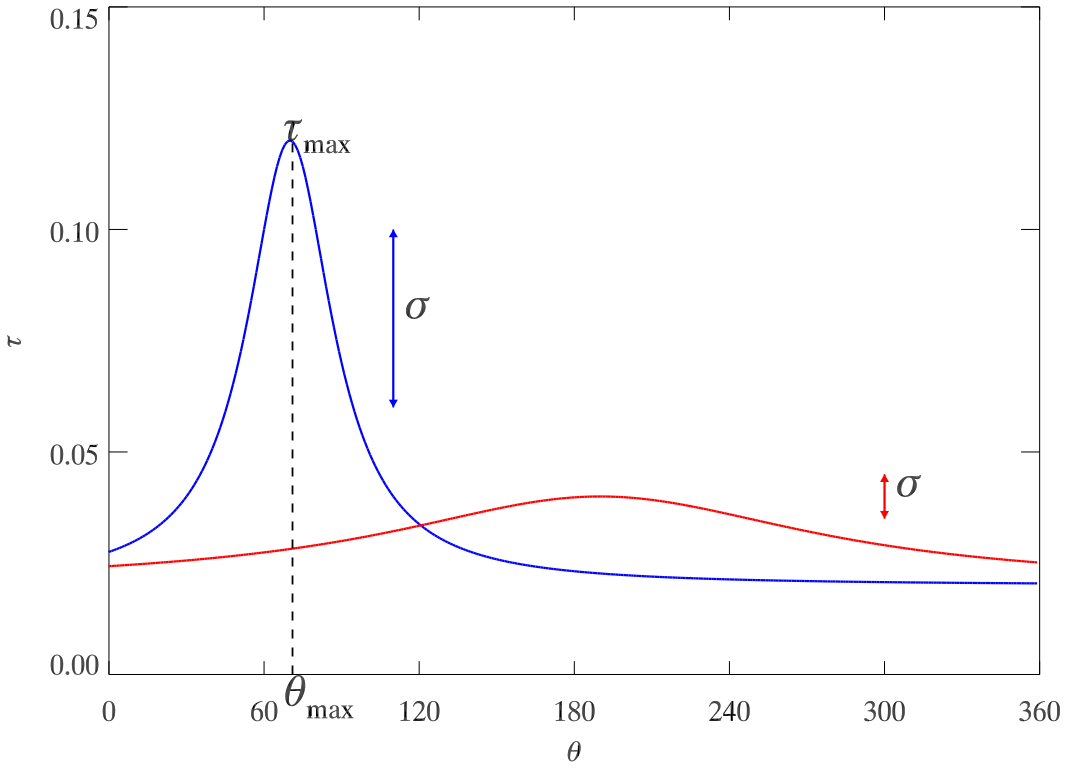

Figure 3.3: For each $1° \times 1°$ point, τ is expressed as a function of wind direction. The blue curve represents represents the case where τ depends strongly on wind direction and so has a large σ_τ. The red curve represents the case where τ does not depend on wind direction and so has a small σ_τ.

The histogram of σ_τ for all global oceanic points is plotted in Figure. 3.3. The main peak in Figure. 3.3 is interpreted as the typical variability of τ as a function of direction. The large tail of high variability denotes aerosol being transported from preferred directions. To differentiate locations with typical τ, from these demonstrating a preferred direction a threshold is being used, σ_τ^{th}, of about 2/3 of the peak values (i.e. a value of 0.035).For any point, if $\sigma_\tau \geq \sigma_\tau^{\text{th}}$, it implies there are possible external aerosol sources other than the ocean itself: this type of point is taken to be non-remote ocean.

It is interesting to look at those points that are identified as being non-remote ocean.

For these points, the corresponding angle $\theta_{\max}$ is found where the averaged τ is maximum. This $\theta_{\max}$ indicates a possible important direction of aerosol transport to the given region.

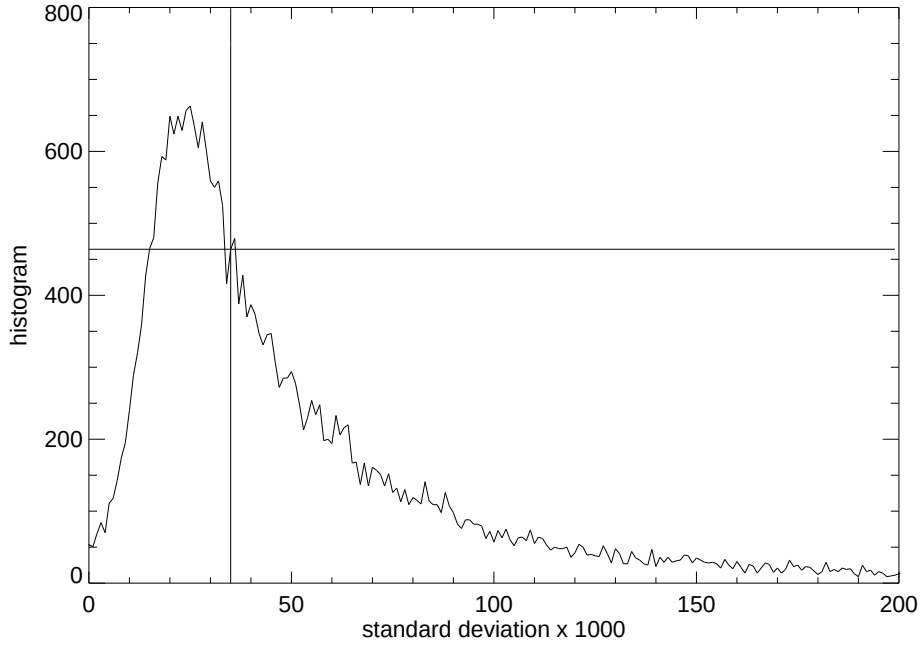

Figure 3.4: Histogram of σ_τ for global ocean points

3.4 Results

A map of $\theta_{\max}$ for the points where σ_τ is greater than σ_τ^{th} is shown in Figure. 3.4, indicating the source direction of transported aerosols for these points.

This map roughly matches the large-scale flow field and storm tracks. For the mid-latitude ocean[$30^\circ - 60^\circ$ N] northern hemisphere, enhanced aerosol loading occurs when the wind direction is westerly, taking heavy - industry pollutants from East Asia and North America.

For the tropical and sub-tropical Atlantic regions, it is obvious that North Africa is a main source of aerosol for the surrounding areas. Over the sub-tropical and tropical Atlantic ocean, the $\sigma_\tau^{\max}$ matches the direction of trade winds that transport dust from the Sahara.

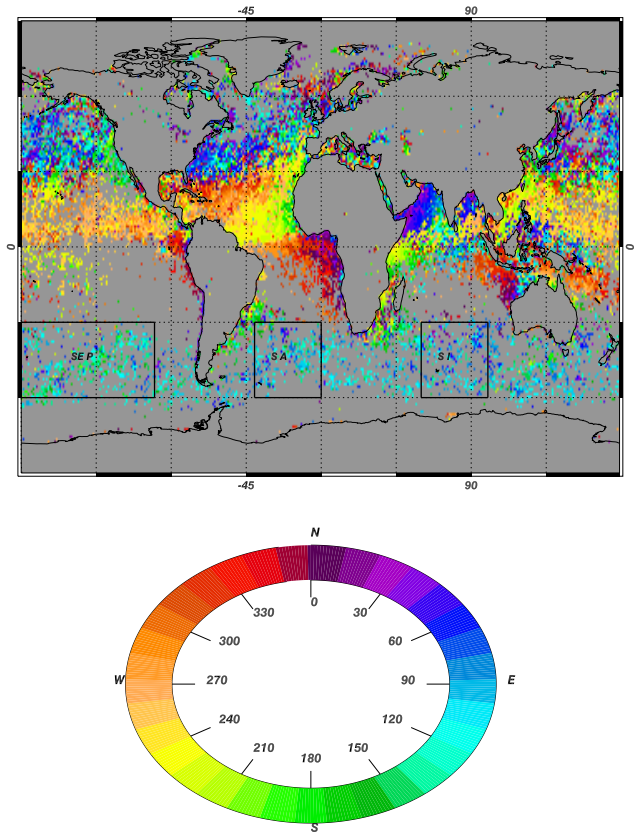

Figure 3.5: Plot of wind direction $\theta_{\max}$ for the locations where σ_τ is greater than 0.035. Rectangular show regions discussed.

The largest value of τ occurs in the Persian Gulf, where wind comes from the south west. For the points located in the east central Pacific, τ is maximum with east wind, indicating that the large values of τ over these points probably relate to long range transport aerosol from biomass burning in South America or dust from the Sahara. Over the west central Pacific, as well as the southern China sea, τ is largest when wind comes from a roughly northerly direction. This could be related to sand storms from northern China and Mongolia.

Over the southern oceans (between $30° - 60°$ S), the largest τ occurs when wind directions are in a range of $70°$ to $140°$. Wind from those directions could be taken as west wind. Since there are no large continents in this region, this zonal region could be thought of as remote ocean region, with little influence from continents. From this map, many regions, especially in the northern hemisphere, could not be regarded as pure remote oceans. This result is supported by the carbon monoxide (CO) distribution map from Measurements Of Pollution In The Troposphere (MOPITT) (see Figure. 3.4). The two main sources for CO are industrial pollution and biomass burning. The high CO in the northern hemisphere indicates that those regions may be influenced by long distance transportation from land while the regions between $30° - 60°$ S have relatively low CO concentrations. Experiments with a long time period (more than one year) aimed at aerosol properties over remote ocean carried out in such regions could lead to unreliable results.

Based on this analysis, remote ocean points over three regions have been chosen, shown in Figure. 3.4. Since they suffer less influence from land, the loading aerosols for these regions are free contamination of long range tranported aerosol, it is easy to detect the link between marine AOD, τ, and wind speed. The relationship between wind speed and τ for the given regions is plotted in Figure. 3.4 to Figure. 3.4. All plots show the similar relationship between wind speed and τ, which is largely linear up to $s = 20$ ms^{-1}. The aerosol optical depth is observed to increase by around 0.1 over a wind speed range of 4 to 20 ms^{-1}. This significant increase can be interpreted to the enhanced contribution of sea-salt particles. Importantly there is no indication that an exponential function is a better fit to the measurements than a straight line. A linear (green line) and an exponential curve (red line) are fitted to the data. Figure. 3.4 shows the average relationship among those three regions. τ over the remote

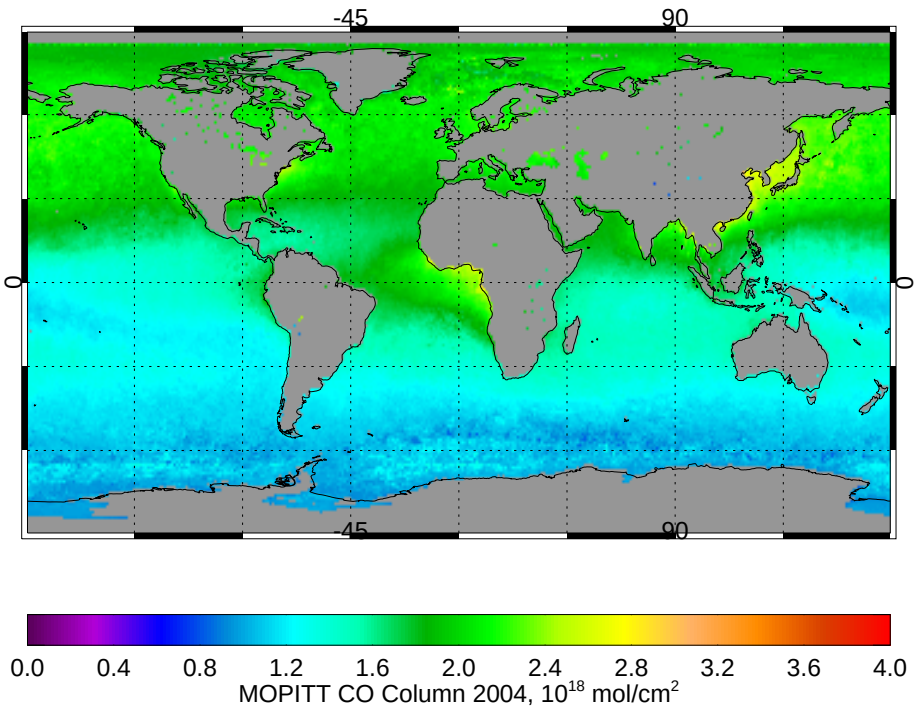

Figure 3.6: Column CO distribution from MOPITT, 2004

oceans increases with sea surface wind speed following a linear relation of the form:

$$\tau = a + b \times s \tag{3.1}$$

where a and b are constants. The gradient b has a value of 0.0040 ± 0.0002 and the offset, a, has a value 0.0850 ± 0.0002. Based on the data of 2003, the similar result is also obtained (Figure. 3.4 to Figure. 3.4). This result is different from Mulcahy et al. [2008] and Glantz et al. [2009], which are taken from the northern Pacific and northern Atlantic respectively, but is very similar with the results of Smirnov et al. [2003] and Jennings et al. [2003], which were taken from Midway Island and Tahiti, which are largely thought to be remote ocean areas due to their long distances from the mainland.

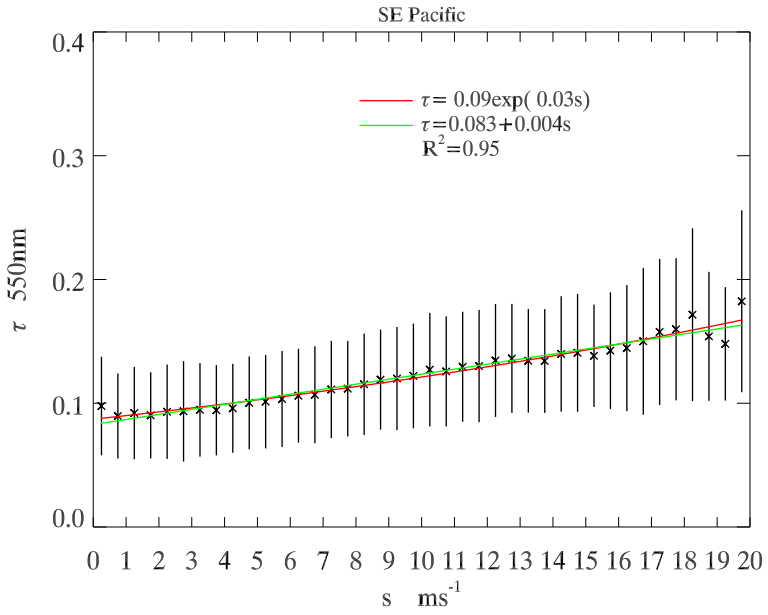

Figure 3.7: Relationship between wind speed and τ over South East Pacific ocean region: 2004

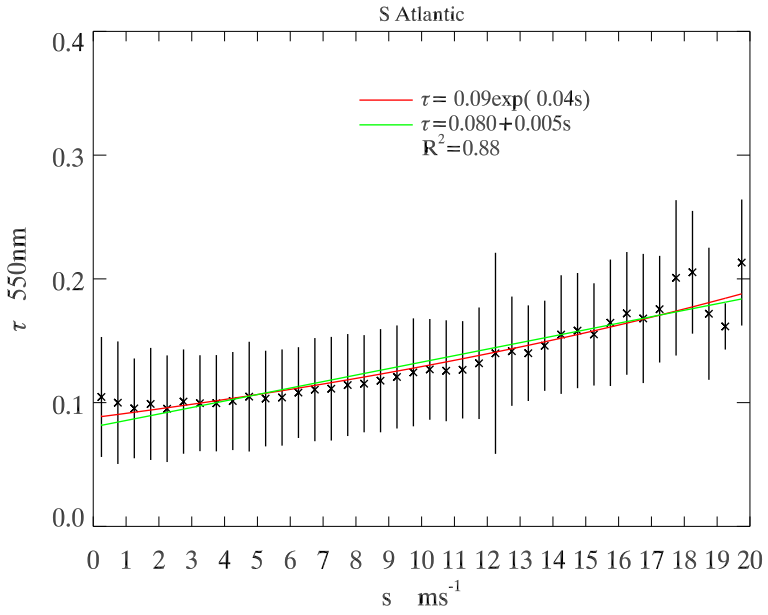

Figure 3.8: Relationship between wind speed and τ over South Atlantic ocean region: 2004

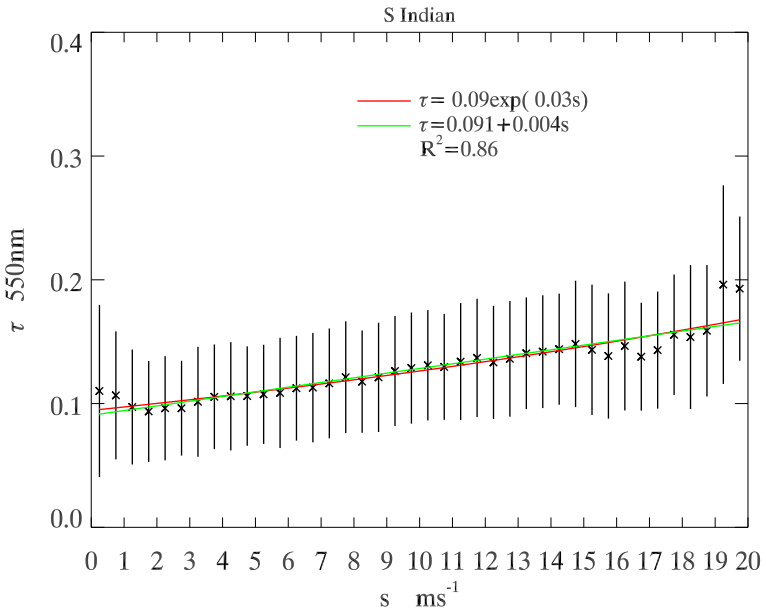

Figure 3.9: Relationship between wind speed and τ over South Indian ocean region: 2004

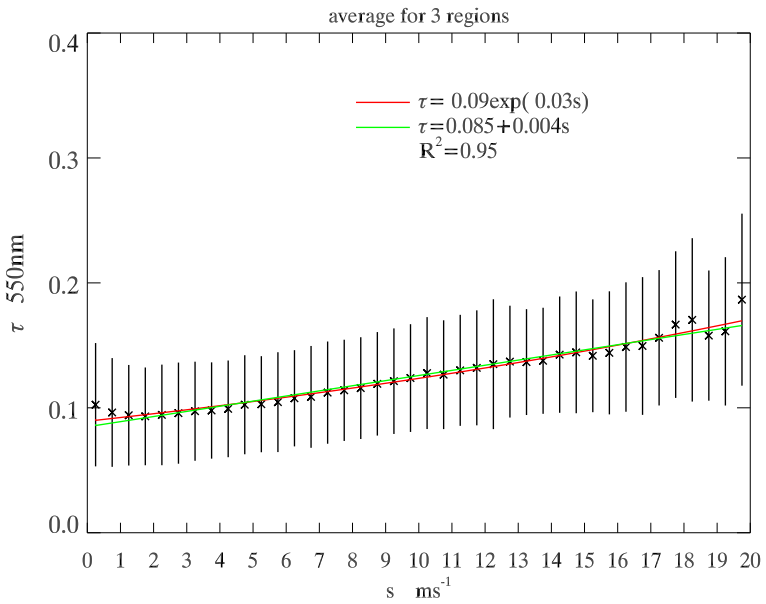

Figure 3.10: Relationship between wind speed and τ over these three regions: 2004

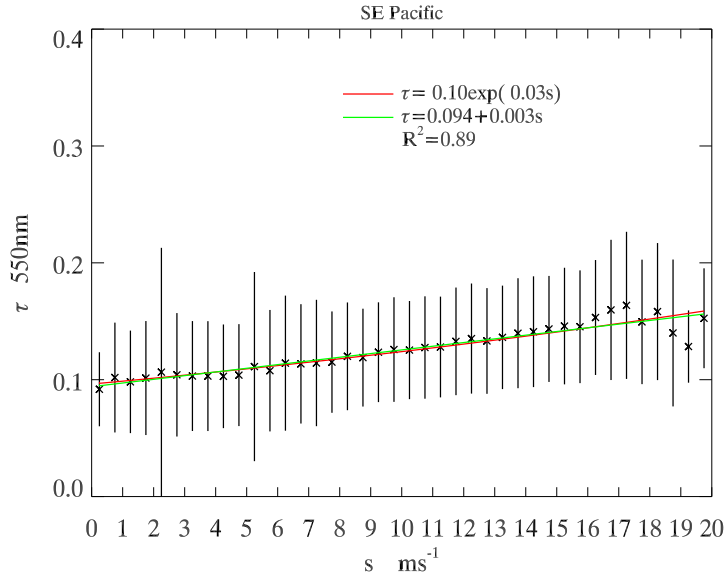

Figure 3.11: Relationship between wind speed and τ over South East Pacific ocean region: 2003

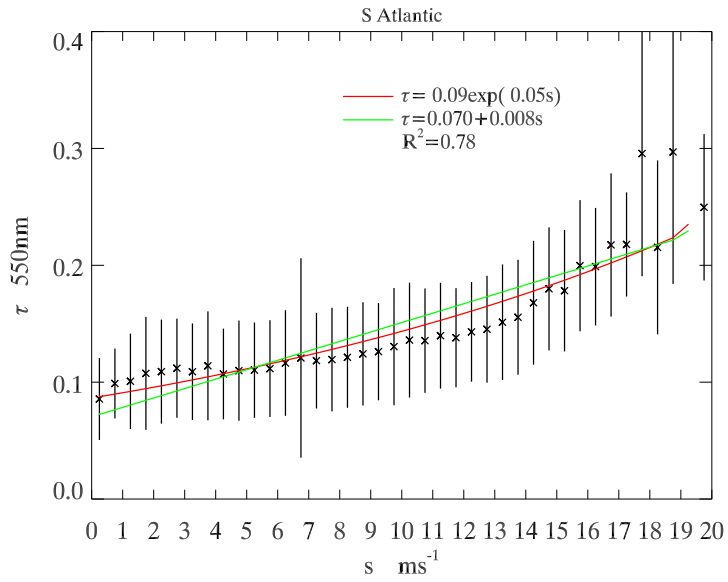

Figure 3.12: Relationship between wind speed and τ over South Atlantic ocean region: 2003

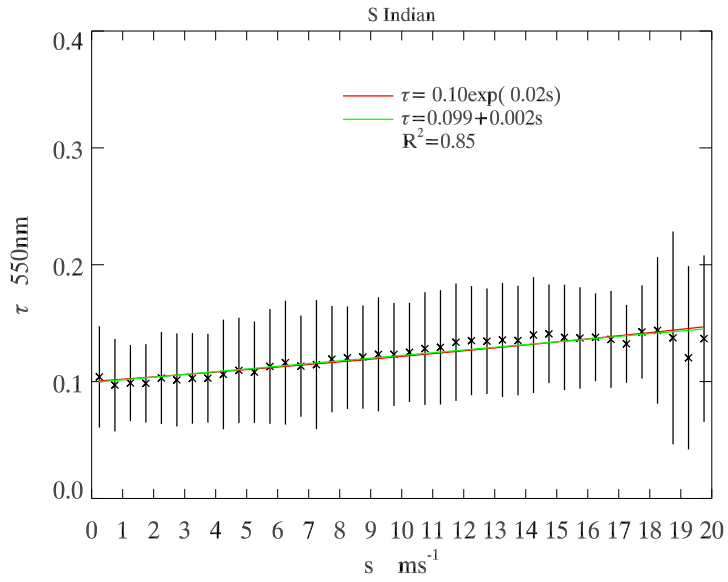

Figure 3.13: Relationship between wind speed and τ over South Indian ocean region:2003

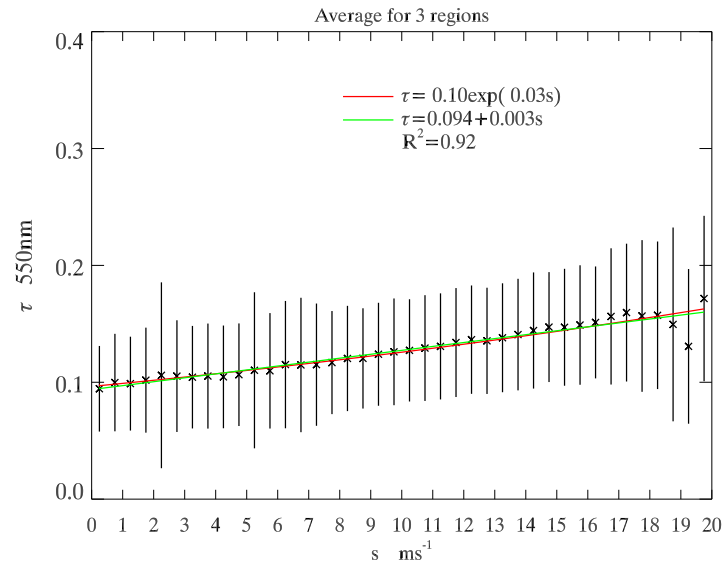

Figure 3.14: Relationship between wind speed and τ over those three regions: 2003

3.5 Conclusions

In this study, the oceanic τ at 550 nm obtained from AATSR has been examined as a function of the surface wind fields from the ECMWF. The remote ocean region is defined by its wind direction and τ. Using this criteria, the majority of the oceans cannot be considered pristine remote ocean, as they show evidence of aerosol transport from land airmasses.

A linear relationship with high correlation coefficients is found between wind speed and τ at 550 nm in clear marine environments, suggesting an important sea-salt contribution to τ. This work extends such a relationship to wind speed of 20 ms^{-1}, higher than in previous studies. This study also shows that under strong wind conditions the τ in clear marine atmosphere could be as high as 0.2 and indicates the important effect of wind speed on the total τ in remote oceans. As the global climate changes, the changing wind pattern could result in significant changes in τ over oceans and could lead to significant changes in τ over oceans and could influence both direct and indirect (via interaction with clouds) aerosol radiative forcing, as well as chemical and biological processes in atmosphere.

Chapter 4

Initial work on SST retrieval

The project of D.Phil. is centered on producing a combined aerosol and surface temperature retrieval by extending the current aerosol algorithm, Oxford-RAL Retrieval of Aerosol and Cloud (ORAC), to the infrared channels of AATSR. Satellite Infrared channels have been used to derive the surface temperature for a long time (Deschamps and Phulpin [1980], Maul and Sidran [1973], Brower et al. [1976]). The radiance at mid-infrared channels also provides more information on large aerosols with effective radius larger than 1 μm, such as desert dust, sea salt and sometimes, volcanic ash. The main objective of design of AATSR is to measure sea surface temperature (SST), with a targeted one sigma accuracy of 0.3 K, according to the requirement of general climate models (Minnett [1990], Zavody et al. [1995]). AATSR provides thermal infrared data at high resolution (1 km) on global scale and like the other satellites, AATSR receives infrared radiance at 3.7, 11 and 12 μm wavelength, in which the effect of the atmosphere is at a minimum. However, the influence of the atmosphere cannot be neglected. In its path through the atmosphere, the radiation leaving surface is significantly modified by the atmosphere in a way which is highly variable in space and time. The AATSR series of instruments view each terrestrial scene at two angles: at nadir and at a forward looking angle of 55°. From two views with different atmospheric path lengths, it is possible to obtain independent information of the atmospheric contribution to the signal at the top of the atmosphere (TOA).

4.1 AATSR SST retrieval scheme

AATSR uses a split window method to correct the effect of atmosphere in the retrieval of SST. SST is retrieved as a linear combination of the brightness temperatures measured in the different channels, BT_i,

$$SST_{ret} = a_0 + \sum_{i=1}^{n} a_i BT_i \tag{4.1}$$

where SST_{ret} is the SST needs to be retrieved, n is the number of channels, i is the index of channel (either from nadir-view only or both nadir and forward and nadir views) (Minnett [1990], Zavody et al. [1995]) and a_0 and a_i are dimensionless coefficients, which are decided by a multiple regression technique using model generated brightness temperatures for a collection of atmospheric profiles.

The principle of the multiple regression technique is to find such values for a_0 and a_i that for the sample used the variance of error (σ^2_{SST}) is a minimum:

$$\sigma^2_{SST} = \frac{1}{m-n-1} \sum_{j=1}^{m} [SST_{ret}(j) - SST_{true}(j)]^2 \tag{4.2}$$

where SST_{true} denotes the sets of SST values used with each atmospheric profile in the generation of brightness temperatures T_i, and m is the number of sample in each latitude region.

The uncertainty in SST given by Equation.
refeqnsig can be contributed by two terms, an atmospheric error σ_{atm}, and instrument noise (σ^2_{ins})

$$\sigma^2_{SST} \propto \sigma^2_{atm}, \sigma^2_{ins} \tag{4.3}$$

The dominant contributors to σ_{atm} are errors due to absorption by gases, variability of aerosol and air - sea temperature difference.

$$\sigma_{atm} \propto \sigma_{gases}, \sigma_{aerosol}, \sigma_{air-sea} \tag{4.4}$$

The algorithm used by AATSR provides a correction for attenuation arising from general gases and background aerosol. In the correction, aerosols are confined in the lowest layer in

the atmosphere, and aerosol extinction (β) is treated as a function of horizontal meteorological range (V) from Koschmieder relationship

$$\beta = \frac{16.99}{V} \tag{4.5}$$

However, for atmospheric conditions with high aerosol loading, especially for the dust aerosol during dust storm seasons, significant bias in SST results from unaccounted effects of aerosol absorption and scattering. This problem has been widely recognized by many satellite-based SST algorithms (Merchant et al. [2006], May et al. [1992], Noyes et al. [2006], Vazquez-Cuervo et al. [2004]), but a global correction from high aerosol loading for AATSR has not been established.

4.2 Sensitivity of brightness temperature (BT) at TOA

4.2.1 Radiative transfer in the atmosphere

The radiance received by a satellite radiometry towards the sea has components originating from the surface, the atmosphere, and the Sun. In the atmosphere, the processes of absorption, emission and scattering are caused by both molecules and aerosols. In the infrared part, the dominant components are (1) the radiation emitted by the surface, but modified by its passage through the atmosphere, (2) the radiation emitted by the atmosphere (including aerosol) into the radiometer field of view and (3) the radiation emitted by the atmosphere (and aerosol) reflected by the sea surface into the radiometer field of view. The radiation from the Sun reflected by the sea surface is negligible comparing with those three factors.

Thus the spectral radiance measured by the satellite at height H above the sea surface $L_H(\lambda)$ can be written as:

$$L_H(\lambda) = \epsilon(\lambda)B(T_s,\lambda)t(\lambda,0,H) + \int_0^H L_A(z,\lambda,T_A)t(\lambda,z,H)dz$$
$$+(1-\epsilon(\lambda))\int_0^H L_A(z,\lambda,T_A)t(\lambda,0,z)t(\lambda,0,H)dz, \quad (4.6)$$

where $\epsilon(\lambda)$ is the emissivity of sea surface at wavelength λ. $B(T,\lambda)$ is the Planck black body radiation function with temperature T, defined as

$$B(T,\lambda)d\lambda = \frac{2hc^2}{\lambda^5}\frac{1}{e^{\frac{hc}{\lambda\kappa T}}-1}. \quad (4.7)$$

where $t(\lambda,0,H)$ is the transmittance of atmosphere from the sea surface to the height H, $L_A(\lambda,z,T_A)$ is the spectral radiance emitted by the atmosphere layer at height z, at a temperature T_A and $t(\lambda,z,H)$ is the transmittance between height z to H. From Equation 4.6, L_λ is a function of atmospheric state and surface temperature. the transmittance t_λ of atmosphere is dependent on optical depth τ_λ, BT can be written as

$$L_\lambda \propto f(T_s,T_A,\tau_\lambda(gases),\tau_\lambda(aerosol),\ldots) \quad (4.8)$$

where f is a function determined by the forward model, T_s is the surface temperature, T_A is the profile of atmospheric temperature, $\tau_\lambda(gases)$ and $\tau_\lambda(aerosol)$ are the optical depths of gases and aerosol.

Radiance measured by AATSR is weighted by the filter response functions, it is necessary to integrate radiance over the width of channel, using the spectral filter response response $\phi_i(\lambda)$ for channel i, to give the channel based brightness temperature L_i. Response functions are different from instrument to instrument.

$$L_i = \frac{\int_0^\infty L_\lambda\phi_i(\lambda)d\lambda}{\int_0^\infty \phi_i(\lambda)d\lambda} \quad (4.9)$$

Figure.4.1 gives the normalized response functions of AATSR 3.7, 11 and 12μm channels. In practice, the intergraded radiance (L_i) is converted to brightness temperature (BT_i): $L_i \longrightarrow BT_i$.

Thus, Equation 4.8 becomes as

$$BT_i \propto f(T_s,T_A,\tau_i(gases),\tau_i(aerosol),\ldots) \quad (4.10)$$

the $\tau_i(gases)$ and $\tau_i(aerosol)$ are optical depth of gases and aerosol at channel i.

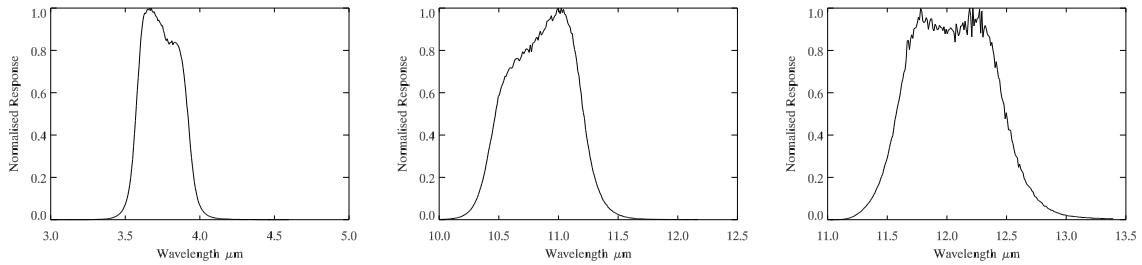

Figure 4.1: The normalized response functions for AATSR, left: 3.7 μm; middle: 11 μm, and right: 12 μm

4.3 Present work: Sensitivity of BT of infrared channels at TOA to atmospheric state

As shown in Equation 4.8, BT_i at TOA relies on the state of atmosphere and surface temperature. It is important to isolate the contributions introduced by aerosol, surface and gases. The present work is to evaluate the effect of absorbing gases to the BT_i at TOA and find out which gases need to be considered in retrieval of aerosol at AATSR infrared channels. The contributions of aerosol will be considered in the future work.

4.3.1 Methodology

The aim of the present work is to figure out which gases matter to the BT_i at the TOA. The main idea is to use a radiative transfer model to simulate the radiance obtained by AATSR using different atmospheric profiles to identify the important gases. Profiles being used are different in surface temperature or concentrations of gases. The radiative transfer model simulates absorption and emission of gases, in fact the gases also have an effect of scattering, but many models do not calculate the scattering process due to the process itself is too complicated.

To start, a criterion to judge the importance of gas is needed. In order to get the required accuracy of SST (δT_s) from AATSR infrared measurement (0.3 K), the accuracy of BT_i at

TOA for each wavelength (δBT_i) has to be achieved. The δBT_i is a complex function of δT_s:

$$\delta BT_i \propto g(T_s, T_A, \tau_i(gases), \tau_i(aerosol), \delta T_s, \ldots) \tag{4.11}$$

The mathematical form of g depends on the particular radiative transfer model used in calculation. The reference state of the atmosphere, including the reference BT_i at the TOA, BT_{i0}, are obtained by feeding a standard atmospheric profile (with standard average amount of gases, temperature, pressure) into the radiative transfer model. The corresponding change (δBT_i) in BT_i is computed by changing the surface temperature by a small number (such as 0.3) while the other factors in the profile are unchanged. The δBT_i is thought to be the variation in BT_i introduced by the change of surface temperature with a reference profile. Inversely, an error of δBT_i at BT_i at TOA would introduce a bias of δT_s to the retrieval of T_s, in order to get a good SST, the accuracy of BT_i has to be better than δBT_i.

The second step is to compute the variation of BT ($\Delta BT_i(gas_{pre})$) at TOA caused by a chosen gas. This is calculated as the difference in BT_i obtained from the standard profile and obtained from the profile that assumes the absence of the very gas with other parameters unchanged. If $\Delta BT_i(gas_{pre})$ is greater than or close to δBT_i, this indicates that this kind of gas could play an important role in the signal of radiance at TOA. It can lead to a significant bias in the retrieval if this gas is neglected, hence the algorithm of retrieval should include the effect of this gas. Otherwise, this gas can be safely neglected.

Finally, the concentration of some particular gases strongly varies with location, height and season (say H_2O and HNO_3). It is also important to know the bias to BT_i caused by the dramatic change in the amount of such a gas. This effect is tested by increasing the concentration of the gas, keeping the other factors unchanged and get the variation of BT ($\Delta BT_i(gas_{var})$) at TOA . The criterion is the same, if ($\Delta BT_i(gas_{var})$) is greater than or close to δBT_i, the variation of this gas influences the BT_i and it is necessary to use a realistic profile for this gas in the retrieval of SST or aerosol instead of utilizing a climatological average values.

4.3.2 Preliminary results

The model being used here is Reference Forward Model (RFM), it is a GENLN2-based line-by-line radiative transfer model developed at the AOPP, Oxford University, under an ESA contract to provide reference spectral calculations for the MIPAS launched on the ENVISAT satellite in 2002. More information can be found at http://www.atm.ox.ac.uk/RFM/.

From the Figure.4.2, produced by A. Dudhia in AOPP, the possible absorbing gases for the aimed channels are found: C_2H_6, CO_2, F12, H_2O, HNO_3, NH_3, O_3, CCL_4, F11, F22. The mid-lat standard atmospheric profile is being used as the reference profile to produce the reference state of atmosphere, including the reference BT_i at TOA. The reference surface temperature is defined as 290 K. It is assumed that the gases are independent from each other. No aerosol is considered in this model. The mixing ratio of gas in mid-lat standard atmospheric profile and one-sigma variation are given in Table.4.1.

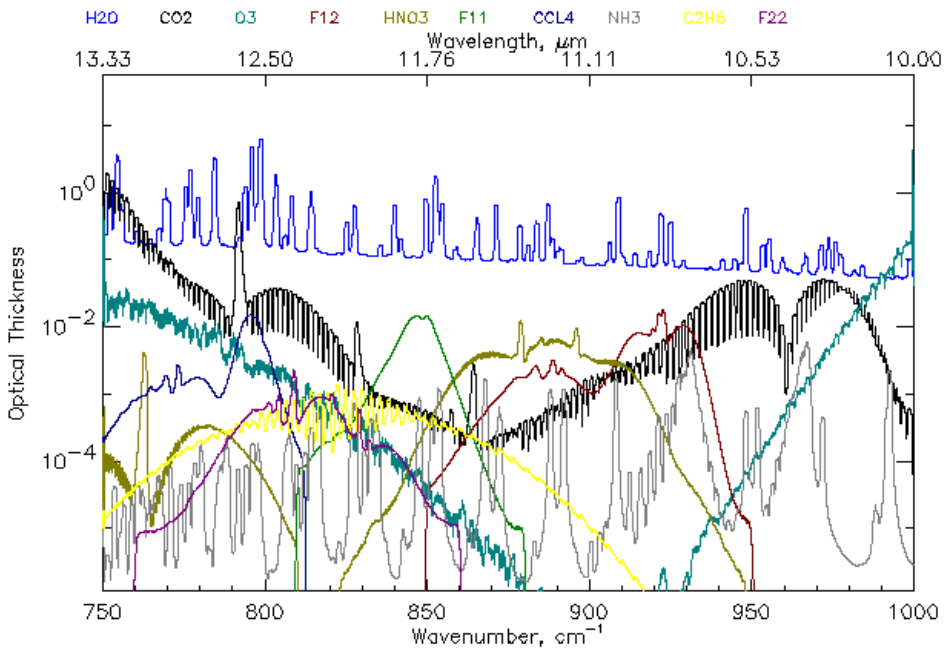

Figure 4.2: Zenith gas optical thickness spectrum, A. Dudhia, AOPP

To get the required accuracy of BT (δBT_i) at each channel, the surface temperature is

Table 4.1: The column mixing ratio of absorption gases of mid-latitude

gas	mixing ratio (ppmv)	one sigma variation (ppmv)	percentage of variation (%)
C_2H_6	0.00015	0.00008	52.937
CO_2	300.26282	9.48663	3.159
F12	0.00011	0.00002	12.246
H_2O	311.80334	269.39740	86.400
HNO_3	0.00087	0.00049	56.383
NH_3	0.00002	0.00005	299.991
O_3	1.7194	0.50907	29.608
CCL_4	0.00001	0.000001	15.317
F11	0.0005	0.00004	7.923
F22	0.0003	0.000003	15.316

Table 4.2: The required accuracy of δBT_i for two views

channel (μm)	view	surface temperature (K)	δT_s (K)	δBT_i (K)
11	nadir	290	0.3	0.285
11	forward	290	0.3	0.278
12	nadir	290	0.3	0.276
12	forward	290	0.3	0.256

increased by δT_s. The result is shown in Table.4.2. Very similar results are also obtained by using difference surface temperatures (280 K, 285 K, 295 K), the possible SST range for mid-lat regions. The variation range of δBT_i from different surface temperatures are within 0.01 K. The required accuracies of 12 μm channel in both views are higher than those for 11 μm channel. For the two channels, the values of δBT_i in forward view are smaller than nadir view. The reason is that the air path of forward view is as nearly 1.75 times long as the path in nadir view. Hence the atmospheric absorption is stronger than that for nadir view, for which higher accuracy is needed to estimate the effect of absorbing gases in the atmosphere.

Based on the obtained criteria for influence of gases for different channels (the first right column of Table.4.2), the importance of each gas can be determined. As mentioned above, to compute the effect of a gas, this gas is intentionally excluded from the reference profile to get a modified profile, e.g. in the modified profile the amount of this gas is 0 and the other

Table 4.3: The contribution of gases to BT ($BT_i(gas_{pre})$) at each channel and view

channel (μm)	view	C_2H_6	CCL_4	CO_2	F11	F12	F22	H_2O	HNO_3	NH_3	O_3
11	nadir	0.0001	0.0000	0.2291	0.0004	0.2500	0.0000	0.5265	0.1213	0.0050	0.0057
11	forward	0.0004	0.0003	0.3824	0.0009	0.4305	0.0003	0.7694	0.2096	0.0088	0.0097
12	nadir	0.00074	0.0135	0.2533	0.1564	0.0056	0.0209	1.6358	0.0427	0.0017	0.0311
12	forward	0.0153	0.0250	0.4015	0.2703	0.0125	0.0385	2.2446	0.0764	0.0057	0.0547

parameters, including surface temperature are unchanged. This modified profile is used as the input for RFM to get a new BT at TOA for each channel (BT_{i1}). The difference between BT_{i1} and BT_{i0}, $\delta BT_i(gas_{pre})$, is thought to be the contribution from this particular gas. The result is shown in Table.4.3.

In the 11 μm channel, the possible important gases for nadir view are CO_2, H_2O, F12, HNO_3 while for forward view are CO_2, H_2O, F12 and HNO_3 The important gases in 12 μm channel nadir view are CO_2, H_2O and F11, for forward view, CO_2 and H_2O, F12 are also important absorbers. As a result, the gases mentioned above should be considered in the retrieval. The effects of O_3 in both views of 12 μm channel are not so strong as the other gases, it should be at the edge of 'importance'.

Although the effects of some gases to BT calculated using their standard average values are not always important, such as HNO_3, their concentrations are highly variable in time and space. Thus their effects would be also change in a wide range. It is important to get the variation of BT_i caused by the variation of gas concentration ($\Delta BT_i(gas_{var})$).

The ($\Delta BT_i(gas_{var})$) is obtained by using sensitivity of BT_i to variation of a gas ($\frac{\partial BT_i}{\partial x}$) times percentage of one-sigma variation of standard amount of this gas (one - σ). x is the percentage of increase.

$$\Delta BT_i(gas_{var}) = \frac{\partial BT_i}{\partial x} \times (one - \sigma) \tag{4.12}$$

The results are shown in Table.4.4—Table.4.7. The only gas whose variation has strong influence to BT at both views of 12 μm is H_2O while for 11 μm channel, H_2O has a strong

Table 4.4: $\Delta BT_i(gas_{var})$ at 11 μm nadir (N) view

11 μm, N	C_2H_6	CO_2	F12	H_2O	HNO_3	NH_3	O_3	CCL_4	F11	F22
$\frac{\partial BT}{\partial x}(K/\%)$	-0.000005	-0.00104	-0.00261	-0.00458	-0.00202	-0.00004	-0.000006	-0.00010	0.00140	0.00021
one-σ var (%)	52.937	3.1595	14.246	86.400	56.383	299.99	29.608	15.317	07.924	09.086
ΔBT (K)	0.00024	0.00329	0.03726	0.39644	0.11407	0.01351	0.00011	0.00153	0.00980	0.00190

Table 4.5: $\Delta BT_i(gas_{var})$ at 11 μm forward (F) view

11 μm, F	C_2H_6	CO_2	F12	H_2O	HNO_3	NH_3	O_3	CCL_4	F11	F22
$\frac{\partial BT}{\partial x}$ (K/%)	0.00001	0.00192	0.00513	0.00680	0.00397	0.00009	0.00001	0.00017	0.00270	0.00040
one-σ var (%)	52.937	3.1595	14.246	86.400	56.383	299.99	29.608	15.317	07.924	09.086
ΔBT (K)	0.00050	0.00608	0.07303	0.58770	0.22424	0.02662	0.00023	0.00260	0.0189	0.00363

influence and the effect of variation of HNO_3 is not as strong as H_2O, but still greater than the other gases. As a result, the retrievals involved with infrared channels should use the realistic profiles for these two gases instead of climatogical data.

Table 4.6: $\Delta BT_i(gas_{var})$ at 12 μm nadir(N) view

12 μm, N	C_2H_6	CO_2	F12	H_2O	HNO_3	NH_3	O_3	CCL_4	F11	F22
$\frac{\partial BT}{\partial x}$ (K/%)	-0.00007	-0.00224	-0.00005	-0.00993	-0.00042	-0.00001	-0.00030	-0.00013	-0.00155	-0.00020
one-σ var (%)	52.937	3.1595	14.246	86.400	56.383	299.99	29.608	15.317	07.924	09.086
ΔBT (K)	0.00384	0.00709	0.00078	0.85827	0.0239	0.00481	0.00897	0.00206	0.01232	0.00189

Table 4.7: $\Delta BT_i(gas_{var})$ at 12 μ m forward (F) view

12 μm, F	C_2H_6	CO_2	F12	H_2O	HNO_3	NH_3	O_3	CCL_4	F11	F22
$\frac{\partial BT}{\partial x}$ (K/%)	-0.00014	-0.00371	-0.00010	-0.01352	-0.00083	-0.00003	-0.00056	-0.00024	-0.00302	-0.00040
one-σ var (%)	52.937	3.1595	14.246	86.400	56.383	299.99	29.608	15.317	07.924	09.086
ΔBT (K)	0.00743	0.01174	0.001551	1.1682	0.04709	0.00934	0.01661	0.00378	0.02400	0.00368

Chapter 5

Ongoing and future work

5.1 Time line and future work

5.1.1 Work to date

- Reacquainting with IDL and FORTRAN.
- Background reading about aerosol properties and retrieval method
- Began with radiative transfer model, RTTOV and RFM.
- Attended academic meeting at Reading
- Studied the AOPP 4th Undergraduate course and completed problem sets as well as examination
- Submitted a paper about wind and aerosol optical depth to Atmospheric Chemistry and Physics

5.1.2 Future work

5.1.3 Absorption in infrared channels

My future work will be a continuation of present work, that is to say, focusing on the influence of gases on the radiance in infrared channels and incorporating their contribution into satellite retrieval algorithm. To be specific, one of the main objectives is to extend current work from a mid-latitude atmospheric profile and fixed reference surface temperature to other common profiles like equator or polar profile for different seasons and different surface temperatures, and take into account the effect of regional and seasonal variation of aerosols. This part of the work is supposed to be finished within next one or two month.

5.1.4 Aerosol retrieval using AATSR infrared channels

Another objective of future work is to modify and extend the ORAC aerosol retrieval algorithm developed by AOPP and RAL, which originally deals with visible and near-infrared data, to include AATSR infrared channels as well as analyze its errors. A similar idea has been developed recently for the inclusion of two infrared channels of SEVIRI (Carboni et al. [2009]). The merit of this work is that for visible channels it is difficult to observe large sized particles above a bright background, while this doesn't obstruct the observation in infrared channels. This work will be involve a great deal of code reading, possibly need about 3 months to finish it.

5.1.5 Optimal estimation for SST retrieval

The ORAC is an optimal estimation (OE) scheme which uses the Levenburg-Marquardt iteration algorithm. The basic principle of optimal estimation is to maximize the probability of the retrieved state based on the value of the measurements and a priori information. Formally, it is required to maximize the conditional probability $P = P(x|y, x_a, b)$ with respect to the values of the state vector x, where x_a is the a priori value of the state vector and b

are all other parameters not modeled by the forward model. This OE frame work allows to characterize the error in each parameter in each individual observation. The state of x includes aerosol optical depth of visible or near infrared, effective radius, surface albedo (Sayer [2008], Thomas et al. [2007]). In the future work, SST will be reprieved using the OE frame.

Thus the state vector x will become as follows:

$$x = [\tau_{aerosol}, SST, R_{nadir}, R_{forward}] \tag{5.1}$$

Unlike the split window technique implicitly assumes an average aerosol correction, in OE frame, aerosol is retrieved as part of the SST retrieval so that changing aerosol values are accounted for. A dynamic aerosol correction can be added to improve the accuracy of SST over the regions with high loading desert dust. This work will take 8 months.

The work in the third year will include to process some papers about validations of the joint aerosol/SST retrieval.

Bibliography

M. O. Andreae and P. J. Crutzen. Atmospheric aerosols: Biogeochemical sources and role in atmospheric chemistry. *Science*, 276:10521058, 1997.

Edgar L Andreas. A new sea spray generation function for wind speeds up to 32 m s1. *Journal of Physical Oceanography*, 28:21752184, 1998.

G. P. Ayers, J. P. Ivey, and R. W. Gillett. Coherence between seasonal cycles of dimethyl sulphide, methanesulphonate and sulphate in marine air. *Nature*, 349:404 – 406, 1991.

R. L. Brower, H. S. Gohrband, W. G . Signore, and C. C. Walton. Satellite derived sea surface temperatures from noaa spacecraft. Technical report, NOAA, 1976.

E. Carboni, G. Thomas, R. Grainger, C. Poulsen, R. Siddans, and A. Sayer. Aerosol retrieval using visible and infrared seviri data. processing, 2009.

R. J. Charlson, S. E. Schwartz, and J. M. Hales. Climate forcing by anthropogenic aerosols. *Science*, 255:423 – 430, 1992.

M. Chin. Tropospheric aerosol optical thickness from the gocart model and comparisons with satellite and sun photometer measurements. *Journal of the Atmospheric Sciences*, 59:461 – 483, 2002.

Mian. Chin, Ralph. A. Kahn, Lorraine. A. Remer, and Hongbin. Yu. Atmospheric aerosol properties and climate impacts. Technical report, NASA Goddard Space Flight Center, 2009.

A. Clarke, V. Kapustin, S. Howell, and K. Moore. Sea-salt size distributions from breaking waves: Implications for marine aerosol production and optical extinction measurements during seas. *Journal of Atmospheric and Oceanic Technology*, 20:1362–1374, 2003.

I. Colbeck. *Physical and Chemical Properties of Aerosols*. Blackie Academic and Professional, 1998.

E. Dahl, 2005. The figure is obtained from the slides made by E. Dahl from State University of New York.

C. Davies. Size distribution of atmospheric particles. *Journal of Aerosol Science*, 5:293 – 300, 1974.

P. Y. Deschamps and T. Phulpin. Atmospheric correction of infrared measurements of sea surface temperature using channels at 3.7, 11 and 12 μm. *Boundary-Layer Meteorology*, 18:131–143, 1980.

Oleg. Dubovik, Brent. Holben, Thomas. F. Eck, Alexander. Smirnov, and Yoram. J. Kaufman. Variability of absorption and optical properties of key aerosol types observed in worldwide locations. *Journal of the Atmospheric Sciences*, 59:590 – 608, 2002.

R. A. Duce, C.K. Unni, B. J. Ray, J. M. Prospero, and J. T. Merrill. Long range atmospheric transport of soil dust from asia to the tropical north pacific. *Science*, 209:1522 – 1524, 1980.

H. J. Exton, J. Latham, P. M. Park, S. J. Perry, M. H. Smith, and R. R. Allan. The production and dispersion of marine aerosol. *Q. Jl. R. Met. Soc*, 111:817–837, 1985.

J. W. Fitzgerald. Marine aerosols: a review. *Atmospheric Environment*, 25A:533–546, 1991.

P. Ginoux, M. Chin, I. Tegen, and J. M. Prospero. Sources and distributions of dust aerosols simulated with the gocart model. *Journal of Geophysical Research*, 160:20255 – 20273, 2001.

P. Glantz, E. N. Nilsson, and W. Hoyningen-Huene. Estimating a relationship between aerosol optical thickness and surface wind speed over the ocean. *Atmospheric Research*, 92:58–68, 2009.

J. L. Gras and G. P. Ayers. Marine aerosol at southern mid-latitudes. *Journal of Geophysical Research*, 88:10661–10666, 1983.

J. Hansen, M. Sato, and R. Ruedy. Radiative forcing and climate response. *Journal of Geophysics Research*, 102:6831 – 6864, 1997.

J. Haywood and O. Boucher. Estimates of the direct and indirect radiative forcing due to tropospheric aerosols: A review. *Review of geophysics*, 38:513 – 543, 2000.

J. Heintzenberg, D. C. Covent, and R. VAN Dongenen. Size distribution and chemical composition of marine aerosols: a compilation and review. *Tellus Series B: Chemical and Physical Meteorology*, 52:1104–1122, 2003.

L. M. Hildemann, G. R. Markowski, and Glen. R. Cass. Chemical composition of emissions from urban sources of fine organic aerosol. *Environmental Science and Technology*, 25: 744–759, 1991.

W. C. Hinds. *Aerosol technology,second edition.* John Wiley and Son., 1999.

W. A. Hoppel, J. W. Fitzgerald, and E. J. Mack. Aerosol size distributions and optical properties found in the marine boundary layer over the atlantic ocean. *Journal of Geophysical Research.*, 95:3659–3686, 1990.

M. Z. Jacobson. Strong radiative heating due to the mixing state of black carbon in atmospheric aerosols. *Nature*, 409:695 – 697, 2001.

S. G. Jennings, C. Kleefeld, C. D. O'Dowd, C. Junker, T. G. Spain, P. O'Brien, A. F. Roddy, and T. C. O'Connor. Mace head atmospheric research stationcharacterization of aerosol radiative parameters. *Boreal Environ. Res.*, 8:303314, 2003.

Yoram. J. Kaufman, Didier. Tanr, and Olivier. Boucher. A satellite view of aerosols in the climate system. *Nature*, 419:215 – 223, 2002.

J. T. Kiehl and B. P. Briegleb. The relative roles of sulfate aerosols and greenhouse gases in climate forcing. *Science*, 260:311 – 314, 1993.

Michael. D. King, Yoram. J. Kaufman, and Didier Tanrand Teruyuki. Nakajima. Remote sensing of tropospheric aerosols from space: Past, present, and future. *Bulletin of the American Meteorological Society*, 80:2229 – 2259, 1999.

M. Kulmala, U. Pirjola, and J. M. Makela. Stable sulphate clusters as a source of new atmospheric particles. *Nature*, 404:66–69, 2000.

Zev. Levin and William. R. Cotton. *Aerosol Pollution Impact on Precipitation: A Scientific Review*. Springer, 2009.

Ernie. R. Lewis and Stephen. E. Schwartz. *Sea Salt Aerosol Production*. American Geophysical Union, 2004.

G. A. Maul and M. Sidran. Atmospheric effects on ocean surface temperature sensing from the noaa satellite scanning radiometer. *Journal of Geophysical Research*, 78:1909 – 1916, 1973.

D. A. May, L. L. Stowe, and J. D. Hawkins. A correction for saharan dust effect on satellite sea surface temperature measurments. *Journal of Geophysical Research*, 97:3611 – 3619, 1992.

R. L. McDonald, C. K. Unni, and R. A. Duce. Estimation of atmospheric sea salt dry deposition: Wind speed and particle size dependence. *Journal of Geophysical Research*, 87(C2):1246, 1982.

C. J. Merchant, O. Embury, P. Le Borgne, and B. Bellec. Saharan dust in nighttime thermal imagery: Detection and reduction of related biases in retrieved sea surface temperature. *Remote Sensing of Environment*, 104:15 – 30, 2006.

P. J. Minnett. The regional optimization of infrared measurements of sea surface temperature from space. *Journal of Geophysical Research*, 95:13497 – 13510, 1990.

K. K. Moorthy and S. K. Satheesh. Characteristics of aerosols over a remote island, minicoy in the arabian sea: Optical properties and retrieved size characteristics. *Q. J. R. Meteorol. Soc.*, 126:81 – 109, 2000.

K. K. Moorthy, S. K. Satheesh, and B. V. K. Murthy. nvestigations of marine aerosols over the tropical indian ocean. *Journal of Geophysical Research*, 102:827–842, 1997.

C. Moulin. Control of atmospheric export of dust from north africa by the north atlantic oscillation. *Nature*, 378:691 – 694, 1997.

J. P. Mulcahy, C. D. ODowd, and S. G. Jenningsand D. Ceburnis. Significant enhancement of aerosol optical depth in marine air under high wind conditions. *Geophysical Research Letters*, 35:L16810–L16813, 2008.

Prabha. R. Nair and K. Krishna. Moorthy. Effects of changes in atmospheric water vapor content on physical properties of atmospheric aerosols at a coastal station. *Journal of Atmospheric and Solar-Terrestrial Physics*, 60:563 – 572, 1998.

E. D. Nilsson, U. Rannik, and M. Norman. Turbulent aerosol fluxes over the arctic ocean 2. wind-driven sources from the sea. *Journal of Geophysical Research*, 106:32139–32154, 2001.

P. R. North. Estimation of aerosol opacity and land surface bidirectional reflectance from atsr-2 dual-angle imagery: Operational method and validation. *Journal of Geophysical Research*, 107:xxx, 2002.

P. R. North, S. A. Briggs, S. E. Plummer, and J. J. Settle. Retrieval of land surface bidirectional reflectance and aerosol opacity from atsr-2 multiangle imagery. *IEEE Trans. Geosci. Remote Sens.*, 37(1):526 – 537, 1999.

E. J. Noyes, P. J. Minnett, J. J. Remedios, G. K. Corlett, S. A. Good, and D. T. Llewellyn-Jones. The accuracy of the aatsr sea surface temperatures in the caribbean. *Remote Sensing of Environment*, 101:38 – 51, 2006.

C. D. O'Dowd and M. H. Smith. Physicochemical properties of aerosols over the north-east atlantic: Evidence for wind-speed-related submicron sea-salt production. *Journal of Geophysical Research*, 98:1137–1149, 1993.

C. D. O'Dowd, Michael H. Smith, Ian E. Consterdine, and Jason A. Lowe. Marine aerosol, sea-salt, and the marine sulphur cycle: a short review. *Atmospheric Environment*, 10: 1352–2310, 2001.

Colin D O'Dowd and Gerrit de Leeuw. Marine aerosol production: a review of the current knowledge. *Phil. Trans. R. Soc*, 365:1753–1774, 2007.

C. M. R. Platt and G. R. Patterson. The interpretation of baseline atmospheric turbidity measurements at cape grim. *Tasmania, J. Atmos. Chem.*, 4:187197, 1986.

J. M. Prospero. Long-term measurements of the transport of african mineral dust to the southeastern united states: Implications for regional air quality. *Journal of Geophysics*, 104:15917 – 15927, 2005.

J. P. Putaud, N. Mihalopoulos, B. C. Nguyen, J. M. Campin, and S. Belviso. Seasonal variations of atmospheric sulfur dioxide and dimethylsulfide concentrations at amsterdam island in the southern indian ocean. *Journal of Atmospheric Chemistry*, 15:117 –131, 2004.

J. S. Reid, P. V. Hobbs, A. L. Rangno, and D. A. Hegg. Relationships between cloud droplet effective radius, liquid water content, and droplet concentration for warm clouds in brazil embedded in biomass smoke. *Journal of Geophysical Research*, 104:61456153, 1999.

L. A. Remer, Y. J. Kaufman, B. N. Holben, A. M. Thompson, and D. P. McNamara. Biomass burning aerosol size distribution and modeled optical properties. *Journal of Geophysical Research*, 103:31879 31891, 1998.

S. K. Satheesh and V. Ramanathan. Large differences in tropical aerosol forcing at the top of the atmosphere and earth's surface. *Nature*, 405:60–63, 2000.

A. Sayer. *Aerosol Remote Sensing Using AATSR*. PhD thesis, Univeristy of Oxford, 2008.

A. Smirnov, Y. Villevalde, N. T. O'Neill, A. Royer, and A. Tarussov. Aerosol optical depth over the oceans: Analysis in terms of synoptic air mass types. *Journal of Geophysical Research*, 16:639–650, 1995.

A. Smirnov, B. N. Holben, O. Dubovik, R. Frouin, T. F. Eck, and I. Slutsker. Maritime component in aerosol optical models derived from aerosol robotic network data. *Journal of Geophysical Research*, 108(D1):1–100, 2003.

G. E. Thomas, S. H. Marsh, S. M. Dean, E. Carboni, R. G. Grainger, C. A. Poulsen, R. Siddans, and B. J. Kerridge. An optimal estimation aerosol retrieval scheme for (a)atsr. Technical report, AOPP,Oxford and RAL, 2007.

G. E. Thomas, C. A. Poulsen, R. Siddans, and A. M. Sayer. Globaerosol : A 12 year global aerosol dataset from european satelllite instruments. *Globaerosol workshop*, 2008.

S. Twomey. *Atmosperic Aerosols*. Elsevier, 1977.

J. Vazquez-Cuervo, E. M Armstrong, and A. Harris. The effect of aerosols and clouds on the retrieval of infrared sea surface temperatures. *Journal of Climate*, 17:3921 – 3933, 2004.

Y. V. Villevalde, A. V. Smirnov, N. T. O'Neill, S. P. Smyshlyaev, and V. V. Yakovlev. Measurement of aerosol optical depth in the pacific ocean and the north atlantic. *Journal of Geophysical Research*, 99:983–988, 1994.

KaMing. Wai and Peter. A. Tanner. wind-dependent sea salt aerosol in a western pacific coastal area. *Atmospheric environment*, 38:1167 – 1171, 2004.

A. M. Zavody, C. T. Mutlow, and D. T. Llewellyn-Jones. A radiative transfer model for sea surface temperature retrieval for the along-track scanning radiometer. *Journal of Geophysical Research*, 100:937 – 952, 1995.